

An evaluation of new particle formation events in Helsinki during a Baltic Sea cyanobacterial summer bloom

Roseline C. Thakur¹, Lubna Dada^{1,2,3}, Lisa J. Beck¹, Lauriane L.J. Quéléver¹, Tommy Chan¹, Marjan Marbouti^{1,12}, Xu-Cheng He¹, Carlton Xavier¹, Juha Sulo¹, Janne Lampilahti¹, Markus Lampimäki¹, Yee Jun Tham^{1,11}, Nina Sarnela¹, Katrianne Lehtipalo^{1,4}, Alf Norkko^{8,9}, Markku Kulmala^{1,5,6,7}, Mikko Sipilä¹, Tuija Jokinen^{1,10}

¹Institute for Atmospheric and Earth System Research/Physics, Faculty of Science, 00014 University of Helsinki, Helsinki, Finland.

²School of Architecture, Civil and Environmental Engineering, École Polytechnique Fédérale de Lausanne, Lausanne, Switzerland

³Laboratory of Atmospheric Chemistry, Paul Scherrer Institute, 5232 Villigen PSI, Switzerland

⁴Finnish Meteorological Institute, Helsinki, Finland.

⁵Aerosol and Haze Laboratory, Beijing Advanced Innovation Center for Soft Matter Science and Engineering, Beijing University of Chemical Technology, 100089 Beijing, China.

⁶Joint International Research Laboratory of Atmospheric and Earth System Sciences, Nanjing University, 210023 Nanjing, China.

⁷Lomonosov Moscow State University, Faculty of Geography, 119991, Moscow, GSP-1, 1 Leninskiye Gory.

⁸Tvärminne Zoological Station, University of Helsinki, J.A. Palméns väg 260, FI-10900 Hangö, Finland

⁹Baltic Sea Centre, Stockholm University, Stockholm, Sweden

¹⁰Climate & Atmosphere Research Centre (CARE-C), The Cyprus Institute, P.O. Box 27456, Nicosia, CY-1645, Cyprus.

¹¹School of Marine Sciences, Sun Yat-Sen University, Zhuhai 519082, China.

¹²Department of Electronics and Nano-engineering, Aalto University, 00076 Aalto, Finland.

Correspondence to: roseline.thakur@helsinki.fi

Abstract

Several studies have investigated New Particle Formation (NPF) events from various sites ranging from pristine locations, including forest sites to urban areas. However, there is still a dearth of studies investigating NPF processes and subsequent aerosol growth in coastal yet semi-urban sites, where the tropospheric layer is a concoction of biogenic and anthropogenic gases and particles. The investigation of factors leading to NPF becomes extremely complex due to the highly dynamic meteorological conditions at the coastline especially when combined with both continental and oceanic weather conditions. Herein, we engage a comprehensive study of particle number size distributions and aerosol-forming precursor vapors at the coastal semi-urban site in Helsinki, Finland. The measurement period, 25 June 2019–18 August 2019, was timed with the recurring cyanobacterial summer bloom in the Baltic Sea region and coastal regions of Finland. Our study recorded several regional/local NPF and aerosol burst events during this period. Although the overall anthropogenic influence on sulfuric acid (SA) concentrations was low during the measurement period, we observed

44 that the regional or local NPF events, characterized by SA concentrations in the order of 10^7
45 molecules per cm^{-3} occurred mostly when the air mass travelled over the land areas. Interestingly,
46 when the air mass travelled over the Baltic Sea, an area enriched with Algae and cyanobacterial
47 blooms, high iodic acid (IA) concentration coincided with an aerosol burst or a spike event at the
48 measurement site. Further, SA-rich bursts were seen when the air mass travelled over the Gulf of
49 Bothnia, enriched with cyanobacterial blooms. The two most important factors affecting aerosol
50 precursor vapor concentrations, and thus the aerosol formation, were speculated to be (1) the type of
51 phytoplankton species and intensity of bloom present in the coastal regions of Finland/ Baltic Sea and
52 (2) the wind direction. During the events, most of the growth of sub-3 nm particles was probably due
53 to SA, rather than IA or MSA, however much of the particle growth remained unexplained indicative
54 of the strong role of organics in the growth of particles, especially in the 3–7 nm particle size range.
55 Further studies are needed to explore the role of organics in NPF events and the potential influence
56 of cyanobacterial blooms in coastal locations.

57

58 Keywords: coastal environment, particle growth, methane sulfonic acid, cyanobacterial summer
59 bloom, sulfuric acid, iodic acid

60

61 **1 Introduction**

62 New particle formation (NPF) and growth of aerosols are regional processes occurring globally
63 introducing a substantial aerosol load into the atmosphere. NPF has been observed in different
64 environments, including pristine (Asmi et al., 2016; Jang et al., 2019; Jokinen et al., 2018), polluted
65 boundary layers and urban areas (Kulmala et al., 2021; Kulmala et al., 2017; Manninen et al., 2010;
66 Kulmala et al., 2016; Wang et al., 2017; Cai and Jiang, 2017; Deng et al., 2020; Yao et al., 2018; Du
67 et al., 2021; Yan et al., 2021), boreal forests (Buenrostro Mazon et al., 2016; Dada et al., 2017;
68 Kulmala et al., 2013; Kyrö et al., 2014; Leino et al., 2016; Nieminen et al., 2014; Rose et al., 2018),
69 tropical forests (Artaxo et al., 2013; Wimmer et al., 2018) and mountain tops (Bianchi et al., 2016,
70 2020). Few studies have investigated NPF processes in a coastal environment although the coastal
71 NPF research started quite early. The investigation of coastal aerosol events dates back to 1978, when
72 the measurements of total aerosol number concentration were carried out at the Tasmanian coast
73 (Bigg and Turvey, 1978). After that atmospheric nucleation was observed in the Southern hemisphere
74 around the Antarctic coastline (O'Dowd et al., 1997), in Mace Head (Flanagan et al., 2005; McFiggans
75 et al., 2004; O'Dowd et al., 2002), in coastal regions of China and Spain (Yu et al., 2019; Mc Figgans
76 et al., 2010; Mahajan et al., 2011) and in open water regions of North East Greenland (Dall'Osto et

77 al., 2018). Most of these studies have identified biogenic emissions from marine algae as the main
78 precursors driving the new particle formation in a perfect coastal setting.

79 The measurements of gaseous precursors, meteorology and biogenic influences are
80 important to study the coastal NPF, which may lead to the formation of coastal/marine clouds. Coastal
81 clouds are the drivers of many coastal ecosystem (Carbone et al., 2013, Emery et al., 2018, Lawson
82 et al., 2018). Any impact or fluctuations in the cloud formation may impact several other processes
83 of the fragile coastal ecosystem. These coastal clouds demonstrate a high sensitivity to CCN (He et
84 al., 2021) and they have a significant impact on the radiation budget because they have a high infrared
85 emission and albedo when compared to the dark water bodies down below. In this study we highlight
86 the type of NPF processes and their drivers in a semi-urban-coastal setting where the atmosphere
87 could be a mixture of anthropogenic and biogenic emissions. Unlike the above mentioned previous
88 studies which were mostly carried out in a perfect coastal environments where NPF would be most
89 likely affected by the biogenic emissions, this study helps to evaluate the impact of urban emissions
90 Vs coastal emissions on NPF and at large the cloud formation processes.

91 It is well documented that sulfuric acid (henceforth SA) is an important precursor to
92 NPF in most environments (Almeida et al., 2013; Kulmala et al., 2013; Croft et al., 2016; Jokinen et
93 al., 2017; Kirkby et al., 2011; Sipilä et al., 2010). The advancement in aerosol research, revealed that
94 a binary system of SA and water is not sufficient to produce particles in ambient atmospheric
95 conditions without stabilizing compounds (Benson et al., 2008; Duplissy et al., 2016; Kirkby et al.,
96 2011). More recently, it has been found that a ternary system involving SA-ammonia-water or SA-
97 amines-water yield much higher nucleation rates as compared to the binary system (Kulmala et al.,
98 2000; Benson et al., 2008; Almeida et al., 2013; Glasoe et al., 2015; Kürten et al., 2016). In addition
99 to these systems, organic compounds which are highly oxygenated - thus less volatile- have been
100 found to contribute to secondary organic aerosol (SOA) mass in forested areas, mountain tops and
101 anthropogenically influenced field sites (Ehn et al., 2014; Pierce et al., 2011; Riipinen et al., 2012;
102 Zhang et al., 2009; Heikkinen et al. 2020; et al., 2020) and laboratory experiments have shown that
103 they can contribute also to the first steps of NPF (Simon et al., 2020; Lehtipalo et al., 2018; Kirkby
104 et al., 2016; Tröstl et al., 2016) .

105 Furthermore, another important molecular class, iodine as well as its related oxidized
106 species play a crucial role in NPF especially in coastal areas (Allan et al., 2015; Mahajan et al., 2009;
107 Raso et al., 2017; Sipilä et al., 2016) and in pristine marine locations (Baccarini et al., 2020; Beck et
108 al., 2021; He et al., 2021). Some previous studies have reported the emissions of I₂ from the
109 macroalgae at coastal sites (Huang et al., 2010; Peters et al., 2005; Saiz-Lopez and Plane, 2004).

110 Several studies from coastal sites like Roscoff, France (Mahajan et al., 2009; McFiggans et al., 2010),
111 Mace Head, Ireland (O'Dowd et al., 2002) and other European coastlines (Mahajan et al., 2011; Saiz-
112 Lopez et al., 2012) have reported iodine species initiating NPF. The reported events can be considered
113 as aerosol burst events with high aerosol concentration and having exceptionally high initial growth
114 rates (GR) (O'Dowd et al., 2002; McFiggans et al., 2004; Mahajan, et al., 2011). The study from the
115 Roscoff coast suggests that the daytime emissions of I₂ produced by macroalgae during low tides
116 drives the particle formation (McFiggans et al., 2010). The iodine oxides and/or oxoacids formed by
117 the biogenic emissions from the micro- and macroalgae near the coastal regions are capable of self-
118 clustering, which could form new particles with a diameter <3 nm and sometimes with a high gas
119 concentration reaching up to 10⁶ cm⁻³ or even more. Recent studies have shown that ion-induced IA
120 nucleation proceeds at the kinetic limit and the overall nucleation rates (ion-induced nucleation +
121 neutral nucleation) driven by iodine oxoacids (IA and iodous acid, HIO₂) are high, even exceeding
122 the rates of well-known precursors of NPF (He et al., 2021b, 2021a): SA with roughly 100 pptv
123 ammonia under similar conditions (Sipilä et al., 2010). The rapid photolysis of I₂, (< 10 s), produces
124 I atoms above the ocean surface and can be detected in high concentrations close to the source region
125 (McFiggans et al., 2010). However, the compounds with longer lifetimes such as CH₃I (two days)
126 provide a source of iodine throughout the troposphere (Saiz-Lopez et al. 2012).

127 Dimethyl sulfide (DMS) oxidation by OH radical in the daytime and by nitrate radical
128 in the nighttime yields other aerosol precursor gases, such as methane sulfonic acid (henceforth,
129 MSA) and SA (Barnes et al., 2006), which play a crucial role in the NPF processes. In a marine
130 coastal environment, MSA concentrations, which are typically lower than those of SA, could be as
131 low as 10% of SA concentration and could maximally reach 100% of SA concentration (Eisele and
132 Tanner, 1993), yet MSA is a potential candidate to participate in the atmospheric nucleation and
133 growth processes (Beck et al., 2021). The stability of heterogeneous MSA clusters have been studied
134 in laboratory and modelling studies (Chen et al., 2020, 2015, 2016) but no study has yet documented
135 MSA clusters in the field. The limited NPF studies in the semi-urban coastal regions and the dynamic
136 coastal meteorology drives the motivation of this research. Another motivation for this research is
137 that, till date no detailed studies on the impact of biogenic emissions on NPF events in Finland were
138 done before in despite the fact that extensive cyanobacteria blooms occur every year in the Baltic
139 Sea region and neighboring water bodies (including Finnish lakes) (Kahru and Elmgren 2014), which
140 could be a significant source of iodine species, SA and MSA. Increasing temperatures and the
141 excessive nutrient load in the Baltic Sea promote algal growth (Kuosa et al., 2017; Suikkanen et al.,
142 2007, 2013). According to HELCOM (Baltic Marine Environment Protection Commission), the
143 Baltic Sea has warmed 0.3° C per decade, however after 1990 significantly faster at 0.6° C per decade

144 and in Finnish coastal areas the warming is even faster with a 2° C increase since 1990 (Humborg et
145 al. 2019). The amount of blue-green algae (i.e. cyanobacteria) has shown a statistically significant
146 increase in open sea areas in the Gulf of Finland, Sea of Åland and the Sea of Bothnia in the last 40
147 years (Kahru and Elmgren, 2014). The increase in frequency and intensity of cyanobacterial blooms
148 would increase the potential emission of biogenic gases changing the composition of the overlying
149 atmosphere and the atmosphere of the neighboring sites, depending on the meteorological conditions.
150 In this semi-urban coastal setting the concentration of gaseous precursors and aerosol size distribution
151 may be influenced by the local meteorological parameters such as wind direction, wind speed, (air
152 mass) turbulences especially at the surface layer of the lower atmosphere. Coastal locations are
153 dynamic environments with rapid changes in meteorological parameters, also making the study of
154 NPF more challenging.

155 In this study, we aim at a thorough evaluation of aerosol precursor molecules with a
156 detailed (NPF events) analysis during the cyanobacterial bloom period, in the coastal-city of Helsinki,
157 Finland, from June to August (summer) 2019..This work evaluates the role of phytoplankton blooms
158 and meteorological parameters in the NPF events observed during the measurement period. We also
159 identify the major precursor vapor(s) and molecular clusters found during the aerosol events. Here,
160 we formulate the hypothesis that gaseous precursors formed from the biogenic emissions from the
161 surrounding marine areas could play an important role in the nucleation processes in Helsinki.
162 Although Helsinki is a coastal area yet the role of marine emissions on NPF processes has not been
163 studied before.

164

165 **2 Measurement Site and Methodology**

166 The measurement sites are surrounded by coastal water bodies (<4km, Vanhankaupunginselkä),
167 forests (<3km) and road connecting to the main city (<300m) as seen in figure 1. Overall Helsinki is
168 located on a relatively flat land on the coast of the Gulf of Finland. The Helsinki Metropolitan area is
169 about 765 km² with approximately one million inhabitants, counting together the city of Helsinki and
170 the neighboring cities of Espoo, Vantaa, and Kauniainen. The climate in southern Finland can be
171 classified as either marine or continental depending on the air-flows and pressure systems. Either
172 way, the weather is milder than typically at the same latitude (60°N) mainly due to the Atlantic Ocean
173 and the warm Gulf Stream.

174



175

176 **Figure 1:** Map showing the two locations included in the study where instruments were operated
 177 (upper left panel). The yellow polygons on the left side of the measurement locations (on the lower
 178 right panel) shows forest/park with little or no traffic (West and Northwest, 300 m from the
 179 measurement site). The yellow double lines on the right of the measurement locations is the traffic
 180 area or the main road (E75) leading to the Helsinki city center (250 m east of the measurement site).
 181 The blue lines depict the coastline after which the lakes and coastal waters of Gulf of Finland start (1
 182 km to the east from the measurement site) © Google Earth 2019

183 The site and measurement period (25 June 2019–18 August 2019) selected for this particular study
 184 are unique since this semi-urban location could be influenced by emissions from the recurring
 185 summertime blooms in the Baltic sea and the neighboring coastal regions. As per the SYKE press
 186 release (2019) the northern part of the Baltic Sea’s main basin, entrance to the Gulf of Finland and
 187 south of the Åland Islands, were enriched with blue-green algae (cyanobacteria). The bloom lasted
 188 from June-August 2019. In coastal areas, bloom was mostly spotted in the Archipelago Sea, Gulf of
 189 Finland, Bothnian Sea and the Quark. The bloom situation developed rapidly and spatially highly
 190 variable, even over short distances. The fragmented nature of the coastal areas and changing wind
 191 and water currents makes the algal bloom conditions highly dynamic.

192 **2.2 Main Instruments**

193 To understand the chemical composition of the precursor vapors emitted from various sources around
 194 the site, the Chemical ionization Atmospheric Pressure interface-Time Of Flight mass spectrometer
 195 (CI-APiTOF) was operated from the 4th floor laboratory of the Physicum building, Kumpula campus,

196 University of Helsinki (60° 12' N, 24° 58' E ; 49m , a.m.sl). The other aerosol and trace gases
197 instruments were operated at the SMEAR III station which is 180 m away from the mass
198 spectrometric measurement site (Station for Measuring Ecosystem-Atmosphere Relation (SMEAR
199 III), 60.20° N, 24.96° E; 25 m a.s.l.).

200 The Atmospheric Pressure interface-Time Of Flight (APiTOF) mass spectrometer is the
201 state-of-the-art instrument for gas phase chemical composition investigations including aerosol
202 precursor characterizations. Here the instrument is coupled with a nitrate based-chemical ionization
203 (CI) inlet in order to measure neutral gas-phase molecules that are clustered and charged with a
204 reagent ion. In our study we used inlet design as described by Eisele and Tanner (1993) and Kurten
205 et al. (2011) and further used by Jokinen et al., 2012. The Time Of Flight (TOF) mass analyzer can
206 detect molecules with masses up to 2000 Th with a mass resolution of 3600 Th/Th. More details on
207 the working principle of the instrument and calibrations can be found in earlier studies (Junninen et
208 al., 2010, Jokinen et al., 2012; Kürten et al., 2014). The sampled air was drawn in through a 1 m-long,
209 “3/4” diameter stainless steel tube with an average flow rate of 10 Lpm. In this study, the chemical
210 ionization was done via nitrate ions (NO_3^-) through X-ray exposure of nitric acid (HNO_3 , flow rate:
211 3 mLpm), saturating the sheath air flow entering the CI (flow rate: 30 Lpm), the inlet flow of 10 Lpm
212 was reached by using a 40 Lpm total flow. The instrument was calibrated prior to the experiment
213 according to (Kürten et al., 2012) resulting in a calibration factor of 1.45×10^9 molecule per
214 normalized unit signal including the diffusion losses in the inlet line.

215 The resulting data (i.e. obtained signals) were averaged to 60 min before the mass
216 calibration step performed through the MATLAB based program tofTools (Junninen et al., 2010).
217 SA, MSA, IA concentrations are calculated after normalizing them with the reagent ions (NO_3^- and
218 $(\text{HNO}_3)\text{NO}_3$) using the equation mentioned in Jokinen et al., 2012. The uncertainty range of the
219 measured concentrations reported in this study is estimated to be $-50\%/+100\%$ and the limit of
220 detection, LOD: 4×10^4 molecules cm^{-3} (Jokinen et al., 2012). HOMs and IA have been estimated to
221 be charged similarly at the kinetic limit as SA (Ehn et al., 2014; Sipilä et al., 2016), so the calibration
222 factor for them should be similar, but please note, that the concentration of other compounds than SA
223 can be highly uncertain due to different ionizing efficiencies, sensitivities and other unknown
224 uncertainties. If MSA, IA or HOMs do not ionize at the kinetic limit these concentrations could be
225 underestimated and thus, the concentrations reported in here should be taken as low limit values. The
226 normalized signals of specific HOMs found in the study are calculated using high resolution peak
227 fitting data. Please note that the concentration of highly oxygenated molecules (HOM monomers and
228 dimers) were calculated from the unit mass resolution data.

229 Neutral cluster and Air Ion spectrometer (NAIS, Airel Ltd., Estonia, Manninen et al.,
230 2010; Mirme and Mirme, 2013) was used to measure the number size distribution of both positive
231 and negative ions between 0.8 nm and 42.0 nm (electric mobility diameter). The NAIS also measures
232 the number size distribution of total particles (neutral) between 2.5–42.0 nm. NAIS consists of two
233 multichannel electrical mobility analyzer columns (DMA's) operating in parallel. The columns differ
234 by the polarity of the ions measured, but are otherwise identical (Mirme and Mirme, 2013) in
235 operation. However they may differ in the transfer functions after calibration. The calibration
236 procedure for the DMAs is presented in Mirme and Mirme, 2013. The ion mode measurements are
237 corrected as in Wagner et al., 2016). The flow rate of the instrument is 60 Lpm which is split into 30
238 Lpm for each DMA. The instrument was installed in the SMEAR III station. The data was recorded
239 every 2 s.

240 Larger particles of 3–820 nm were measured using a twin differential mobility particle
241 sizer (DMPS) (Aalto et al., 2001). The instrument was installed in the SMEAR III station. The time
242 resolution of data is 10 minutes.

243 The size distribution of 1–3 nm particles was measured by a Particle Size Magnifier
244 (PSM, Airmodus Ltd., Finland; Vanhanen et al., 2011) in series with a condensation particle counter
245 (Airmodus Ltd., Finland). The PSM was operated by scanning the flow 0.1–1.3 lpm (continuously
246 changing the saturator flow rate) which allows determining the 1–3 nm particle concentration and
247 calculation of particle size distribution. The data was recorded for each second and the duration of
248 each scan was fixed to 240 s. The raw data inversion was carried out through the kernel method
249 (Chan et al., 2020; Lehtipalo et al., 2014). The raw data of the PSM employed a pretreatment filter
250 that calculates the correlation between the observed particle concentration and the saturator flow rate
251 of a single scan and discards scans with significant non-correlation or negative correlation (Chan et
252 al., 2020). Details about the Back-trajectory calculations, Chl a data analysis, meteorological and other
253 calculations of parameters such as growth rates and formation rates are explained in the SI.

254

255 **3. Results and discussions**

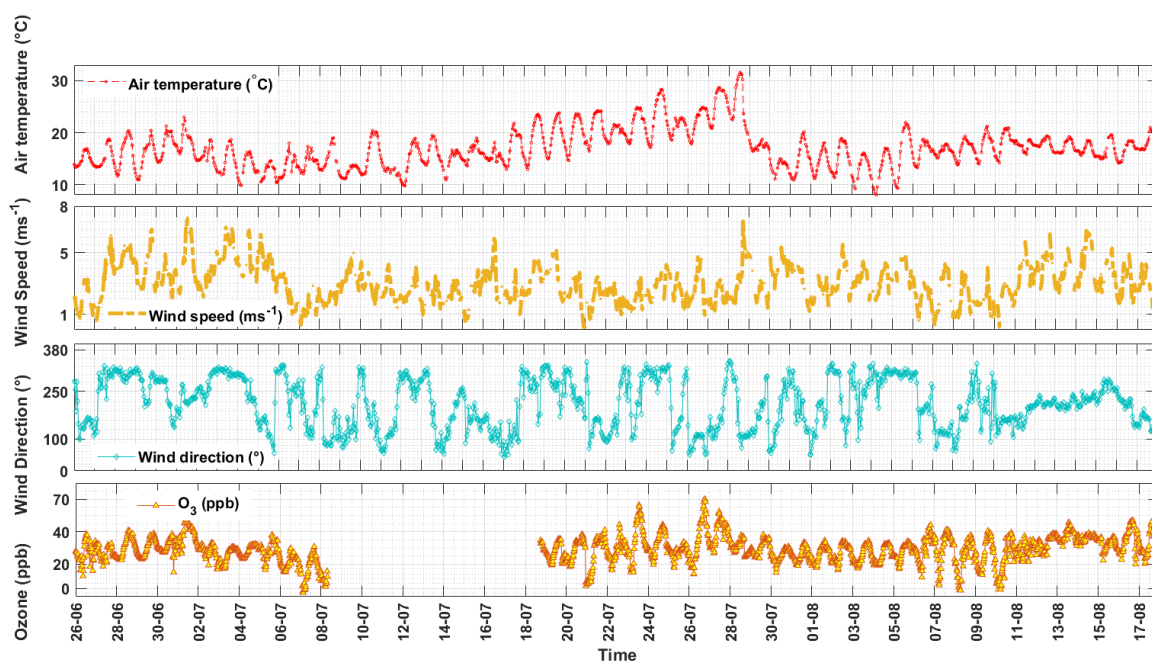
256 **3.1 Meteorological parameters and cyanobacterial bloom during the study.**

257 **3.1.1 Meteorological Parameters**

258 The meteorological parameters, especially the wind speed, wind direction and ambient temperature,
259 varied significantly during the study period. The time format in the entire study is UTC+02:00 h. This
260 study period includes the hottest summer days of Finland in year 2019. The average temperature
261 during 17–28 July (the warmest period) was 21.6° C with a maximum temperature of 31.6° C recorded

262 on the 28 July (Fig. 2). Temperature starts to decrease after 29 July. The average temperature in
263 August was 16.5° C with a maximum temperature of 21.9° C recorded on 5 August 2019.

264 The wind direction was highly variable during June-July period. The wind direction in
265 July was mostly from the sectors 270°–320° (West-Northwest) and 90°–150° (East-South East). In
266 August, the wind gained more stability and was dominantly blowing from 180°–270° (South-West)
267 (Fig. 2). The wind speed also showed high variability in June-July. The wind speeds during June and
268 early weeks of July were mostly $>6.5 \text{ m s}^{-1}$, followed by a bit calmer mid-July (mostly $\leq 4 \text{ m s}^{-1}$)
269 with preceding high winds in end of July until mid-August (gusts of winds $> 5.2 \text{ m s}^{-1}$) (Fig. 2).
270 However, the average wind speeds in both the months was 3 m s^{-1} . The average daylight hours in July
271 were 17-18 hours with the daytime hours between 04:00–22:00 h which starts to decrease in August
272 to 15–16 hours of daylight per day (05:00 h – 21:00 h) as per the Global radiation data obtained from
273 SMEAR III station for the study period. Therefore, the actual nighttime hours in our measurement
274 site can considered from 23:00 h–03:00 h during Finnish summers.



275
276 **Figure 2:** Time series of meteorological parameters and O₃ (data from SMEAR III station, 30-minute
277 averaged) during the study period.

278 279 3.1.2 Cyanobacterial bloom conditions during the study

280 The Baltic Sea (defined from 53° N to 66° N latitude and from 10° E to 30° E longitude inclusive of
281 Gulf of Bothnia, Gulf of Finland and Gulf of Riga) is characterized by usually two algal blooms
282 occurring in early Spring (mostly diatoms) and a summer bloom increasingly dominated by
283 cyanobacteria (blue green algae). The summer bloom period selected for this study was typically

284 characterized by cyanobacteria. When these microscopic cyanobacteria multiply and aggregate, they
285 are seen as blue-green patches or scum-like layers over the surface of lakes and marine waters. The
286 warm early summer temperatures (during June) resulted in a cyanobacterial bloom (Finnish national
287 monitoring; SYKE press release, 2019). However, the weather conditions in end of July began
288 changing with high winds causing the cyanobacteria to be highly mixed in the water column, which
289 reduced bloom intensity at the sea surface to lower than normal mean cyanobacterial biomass (mean
290 biomass of cyanobacteria, $105 \mu\text{g L}^{-1}$, Kownacka et al., 2020) in end of July and August (SYKE press
291 release, 2019). However the average biomass of cyanobacteria in 2019 ($196 \mu\text{g L}^{-1}$, Kownacka et al.,
292 2020) was slightly higher than the average. Subsequently, temperatures were lower in August as
293 compared to June and July and windier as compared to other summer months. These windy conditions
294 kept the lake cyanobacteria well mixed in the water. The northern Baltic Sea, including the Gulf of
295 Finland, the Southern parts of the Åland islands and even the Bothnian Sea occasionally observed
296 massive blooms of cyanobacteria during June-August 2019. However, the bloom intensity of
297 cyanobacteria at the coastal areas were intermittent and changed rapidly due to the spatial complexity
298 of the coastline and variable winds and currents.

299 These cyanobacterial blooms are generally dominated by three taxa, *Nodularia*
300 *spumigena*, *Aphanizomenon* sp. and *Dolichospermum* sp. (Knutson et al., 2016; Kownacka et al.,
301 2020). In the Baltic Sea, these cyanobacteria actually contribute the most to the total pelagic nitrogen
302 fixation (Klawonn et al., 2016). Other potential primary producers emitting vapors are the littoral
303 macroalgae growing along the shallow coastline. For example, the perennial macroalgae, *Fucus*
304 *vesiculosus* covers large areas of the coastal areas of Baltic Sea, where they support very high biomass
305 and high productivity (Attard et al., 2019). Low sea levels (0.2–0.8 m, wave height at Suomenlinna
306 aaltopoiju station, <https://en.ilmatieteenlaitos.fi/wave-height>) were recorded in mid-July (11 July
307 2019–27 July 2019) during the period when high temperatures (20°C and above) prevailed (Fig.2)
308 in our study region. During these conditions, contributors to emissions might be a mix of both coastal
309 macroalgae and open sea microalgae, which are mostly the cyanobacteria. There is a possibility that
310 reasonably, large extents of coastal macroalgae, including *F. vesiculosus*, were exposed to direct
311 sunlight (in shallow waters or low tide conditions) during the decay of the blooms during mid-August
312 (when the bloom intensity was low, SYKE press release, 2019), hence making this time window
313 favorable for observing potentially high emissions in gas phase from macroalgae, in addition to the
314 emissions from cyanobacterial blooms. However, in the semi-urban/coastal setting of this
315 measurement site, there could be various other parameters, which also could play a role in
316 determining the concentrations of the biogenic emissions; for example the wind speed and wind
317 direction. The atmosphere in this semi-urban coastal location is itself a cocktail of various vapors,

318 oxidants and particles, which would affect the quantification, source apportionment and
319 characterization of the biogenic emissions.

320

321 **3.2 Precursor vapor concentrations and their sources**

322 The measured daytime precursor vapor concentrations showed a regular diurnal cycle consistent with
323 the photochemical production of SA and IA in 90% of the days in this study. SA, key precursor of
324 atmospheric NPF, is formed mainly by reaction of sulphur dioxide with OH-radicals, which is
325 predominantly controlled by the photochemical cycles (Sipilä et al., 2010; Jokinen et al., 2017). The
326 daily mean concentration of SA in July and August were almost similar, $\sim 3 \times 10^6$ molec. cm^{-3} . The
327 mean concentration is slightly lower as compared to the concentrations of SA measured in Helsinki
328 street canyon, 1×10^7 molec. cm^{-3} (Olin et al., 2020) but similar to the SA concentration measured at
329 the SMEAR III station in 2018 (Okuljar et al., 2021). In the study of Olin et al., 2020, SA
330 concentrations were greatly affected by vehicular traffic as the site is situated at a busy street canyon.
331 The SMEAR III is considered as a background site much less affected by vehicular traffic (Okuljar
332 et al., 2021). In comparison to other locations, the daytime SA concentration in pristine Antarctic
333 region has been reported from 10^5 up to 10^7 molec. cm^{-3} (Mauldin et al., 2001, Jokinen et al., 2018),
334 10^6 molec. cm^{-3} in remote continental, remote marine and forest regions and 10^7 molec. cm^{-3} in urban
335 and rural agricultural lands using the same technique as in here (Berresheim et al., 2000; Kuang et
336 al., 2008; Petäjä et al., 2009; Kurtén et al., 2011; Zheng et al., 2011; Chen et al., 2012; Jokinen et al.,
337 2012; 2017, Kürten et al., 2014; Bianchi et al., 2016; Baalbaki et al., 2021; Dada et al., 2020). It has
338 been well documented that SA contributes to aerosol formation and growth processes (Boy et al.,
339 2008; Eisele et al., 2006; Fiedler et al., 2005; Iida et al., 2008; Sarnela et al., 2015; Jokinen et al.,
340 2018; Kürten et al., 2015, 2016; Mauldin et al., 2001; Paasonen et al., 2010; Wang et al., 2011; Weber
341 et al., 1998, 1999; Yao et al., 2018; Dada et al., 2020). Most of these studies are conclusive that SA
342 concentration in the atmosphere depends on the anthropogenic and biogenic activities around the site.

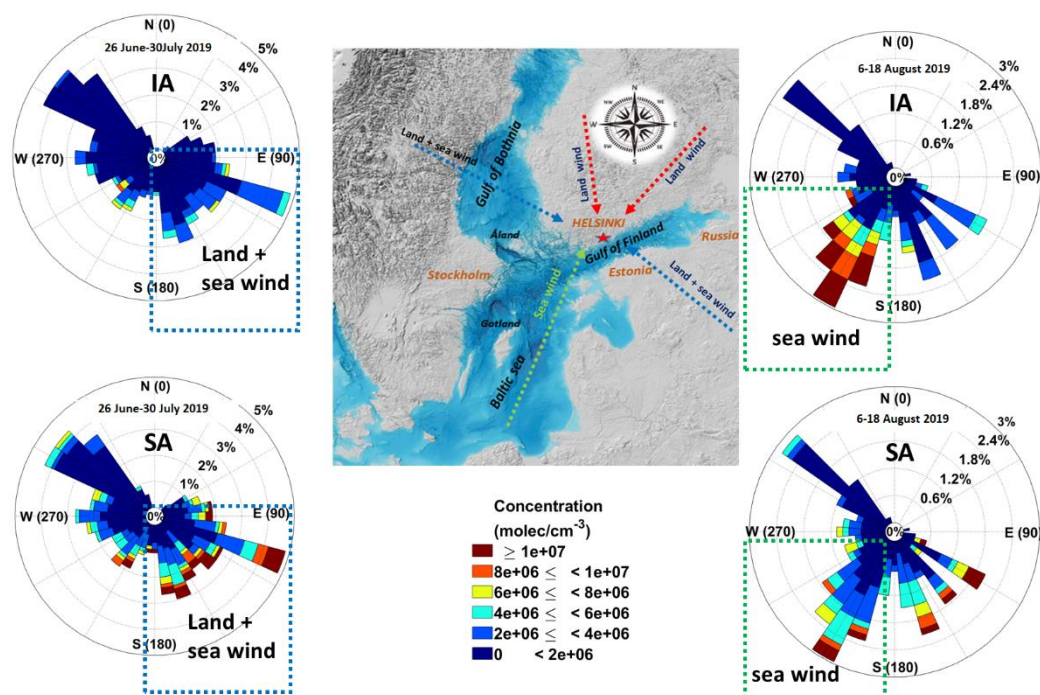
343 In the coastal marine boundary layer, the MSA concentration is typically 10–100% of
344 that of SA (Berresheim et al., 2002; Eisele and Tanner, 1993). Until recently, no studies have been
345 found to report MSA and IA concentrations in coastal/urban setting of Finland. The daily mean
346 concentration of MSA in July and August was almost similar, 4×10^5 molec. cm^{-3} . The mean
347 concentration of IA in July and August was 1×10^6 molec. cm^{-3} and 3×10^6 molec. cm^{-3} , respectively,
348 showing two times increase in IA concentrations in August (Fig. S1). A similar increase in IA
349 concentrations from summer to autumn were observed in the Arctic Ocean, where the increase in IA
350 was attributed to the freezing onset of the pack ice and increase in ozone concentrations (Baccarini et
351 al., 2020). However, here the increase is mainly due to the change in the air mass arriving at the

352 experimental site, enriched with biogenic emissions from the blooms. For the same period, the CI-
353 APiTOF data shows exceptionally high concentrations of highly oxygenated organic molecules
354 (HOMs), with monomer concentrations (300–450 amu) of 10^8 molec.cm⁻³ and HOM dimer
355 concentrations (450–600 amu) of 10^8 molec.cm⁻³ as well (Fig.S2).

356 The IA concentration rises one order of magnitude, from 10^6 to 10^7 during the 11–17
357 August, when the wind direction changes abruptly (from 280°–360° to 180°–230°, marine air mass,
358 Fig. 3). We found that during the marine air (180°–230°, South Easterly, over Gulf of Finland and
359 South westerly, over Northern Baltic sea) influence over the study region the average noontime
360 maximum of SA, IA is on the order of 10^7 molec.cm⁻³ and MSA is around 10^6 molec.cm⁻³ (Fig. 3).
361 This is one order of magnitude higher concentration than when the wind was from over land (Fig. 3).

362 The highest concentration, 3×10^7 molec. cm⁻³ of IA was observed when the wind is
363 coming from the Baltic sea sector, whereas the highest SA concentrations ($\sim 3 \times 10^7$ molec. cm⁻³) was
364 observed when air mass travelled over the countries of Estonia and Russia crossing Gulf of Finland
365 before entering the measurement site (land+sea region). The connection between the aerosol
366 precursors and the wind direction can be observed in the cases where the wind direction changes
367 rapidly. The highest IA concentration was recorded when the wind direction changes after the 4
368 August, 180°–230° (the Baltic Sea region). The change in wind direction was clearly reflected in a
369 reversal of the concentration trends of SA and IA (Fig. 3). It was observed that the winds coming
370 from 80°–180° or 250°–280° (land-sea region, Fig. 3) were SA rich air masses. This comprises of the
371 landmasses of south and northeastern Finland, Northern Russia, part of Gulf of Finland and Estonia
372 and North-North western part of Finland including a part of northernmost Gulf of Bothnia. The sector
373 0°–90° or 280°–360° (land, Fig. 3) consists mostly of urban cities.

374

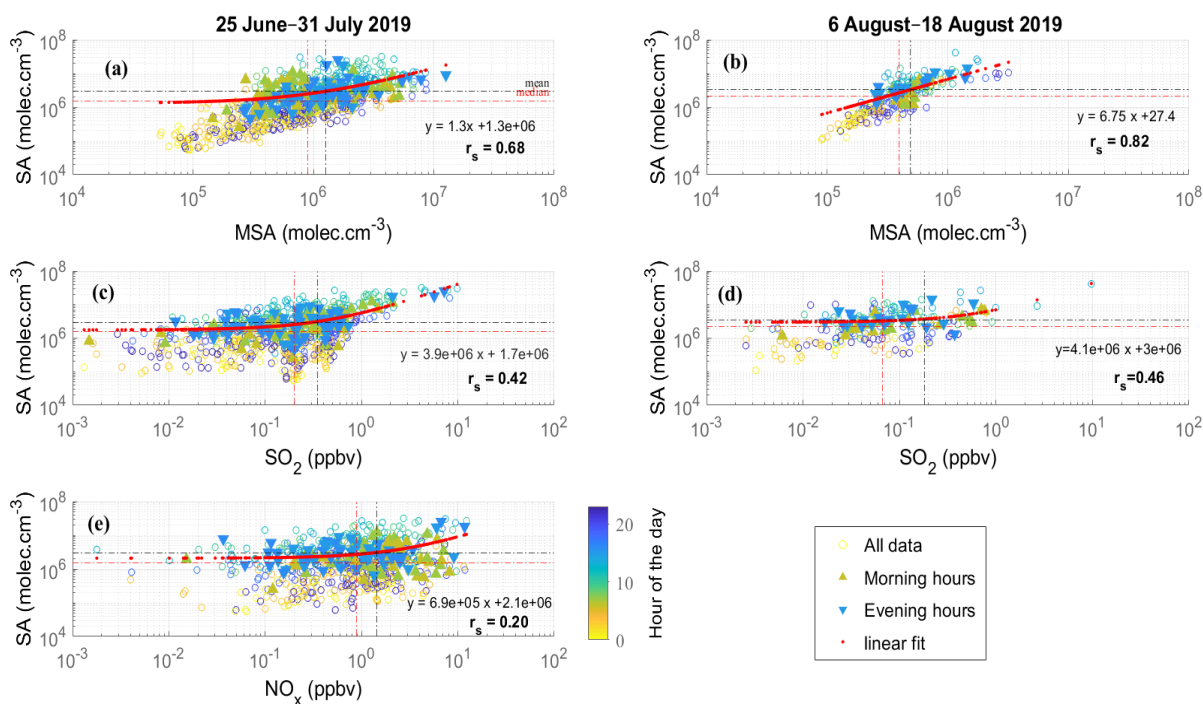


375

376 **Figure 3:** Windroses showing the variability in the concentration of gases with wind direction during
 377 the study period. Percentages on the concentric circles denote the frequency of winds from different
 378 directions. The spokes are color coded as per the concentration of the gas from the particular direction.
 379 The numbers in the parenthesis within the windroses refer to the wind direction in degrees.

380

381 During the entire study period, when the air plume passed over the northern Baltic Sea region and the
 382 wind speed was high enough ($> 4\text{ m s}^{-1}$) high concentrations of IA was observed. While IA can be
 383 exclusively sourced from the marine and biogenic emissions (Mahajan et al., 2011; O'Dowd et al.,
 384 2002; Sipilä et al., 2016; Carpenter et al., 2021), SA could be biogenic or /and anthropogenic. Further,
 385 the temperatures prevailing during this period may have facilitated the DMS oxidation at a higher
 386 rate, which forms the source of biogenic SA and MSA. However, this is not a very simple equation,
 387 since this fractional yield of biogenic SA from DMS oxidation additionally also depends on the
 388 atmospheric NO_x ($\text{NO} + \text{NO}_2$) and HO_x ($\text{OH} + \text{HO}_2$) levels and on the scavenging of SO_2 by sea salt
 389 or cloud droplets (Hoffmann et al., 2016). The anthropogenic sources of SA for this site could also
 390 include vehicular or ship traffic especially considering that there is a city road just 250 m and a harbor
 391 6 km away from the measurement site. We explored the correlations of SA to a biogenic proxy, MSA
 392 and correlation with NO_x (anthropogenic proxy) to have a clear source apportionment of SA (Fig.4).
 393 SO_2 could not be treated entirely as anthropogenic proxy as it can be sourced from DMS oxidation as
 394 well.



395

396 **Figure 4:** Correlation of SA with MSA (a,b), SO₂ (c,d) and NO_x (e) for June–July. The black dashed
 397 lines for both axis represent the mean of the gas concentration, red dashed line represent the median
 398 value the gas concentrations and red solid line represents the linear fit. Spearman's coefficient (r_s)
 399 was used to test the correlation, at significance level, 0.001. The circles represent data points at
 400 different hours of the day. The upward pointing green triangles represent the morning rush hours
 401 (6:00–8:00 h) and the downward pointing blue triangles represent the evening rush hours (15:00–
 402 17:00 h). The yellow hollow circles represent all data. NO_x data unavailable of August.

403

404 The good correlations (r_s > 0.6, Fig. 4a and 4b) between SA and MSA during the study period
 405 (June–August) could suggest that they were sourced from a common biogenic source, the DMS
 406 emission from the cyanobacterial bloom. Good correlations of SA and MSA was also found in August
 407 (r_s = 0.8, Fig. 4b) when the air mass was mostly marine (and/or from the Finnish coastline, Fig. 3).
 408 Another observation was that SO₂ also shows some correlations with SA in both June-July and August
 409 study periods (r_s = 0.4, Fig. 4c and 4d), but not as significant as SA and MSA correlations. SO₂ can
 410 have different sources unlike MSA which is mostly biogenic. However some emissions could be
 411 sourced from agriculture and other terrestrial sources, Bates et al., 1992, hence these observations
 412 could possibly indicate SA was more biogenic than from other sources. But we cannot be very
 413 accurate in this estimation only by analyzing the correlation coefficients since both MSA and SA can
 414 have a similar daily cycles due to the oxidation pathways.

415 Both SO₂ and MSA are the oxidation products of DMS (produced by phytoplanktons, including
416 some cyanobacteria), oxidized through OH and NO₃ radical (Chen et al., 2000). Some of the previous
417 chamber studies have confirmed that SO₂ is the major intermediate products formed from DMS
418 oxidation (Sørensen et al., 1996; Berresheim et al., 1995). The SO₂ could be oxidized to SA (OH/O₂
419 oxidation) during the transport. Since our experimental site was surrounded by water bodies and the
420 summer season had enriched most of these freshwater and marine waters with abundant
421 cyanobacterial blooms, this biogenic SA contribution to the study site has to be accounted when
422 analyzing the sources of SA. However, SO₂ can also be sourced from various anthropogenic activities
423 and can be oxidized to SA. In Finland the major sources of anthropogenic SO₂ is the public power
424 industries contributing to almost 90% to the total SO₂ emissions in Finland in the year 2019, while
425 transport contributing to less than 1% according to the emission inventory prepared by Finnish
426 Environment Institute, SYKE (Finnish Air Pollution Inventory; [ymparisto.fi/en-
427 US/Maps_and_statistics/Air_pollutant_emissions](http://ymparisto.fi/en-US/Maps_and_statistics/Air_pollutant_emissions)). Further the maximum data points of high
428 concentrations of SO₂ ($\sim 10^7$ molec. cm⁻³) were not observed during the traffic hours in June-July-
429 August (Fig. 4c and 4d) another possible indication that biogenic sources could be contributing to the
430 SO₂ concentrations and thus SA concentrations near the study site.

431 The emission inventory of Finland for the year 2019 indicated that sources of NO_x as NO₂ were
432 mainly the power industries (41.5%) and the transport sources (41%) ([ymparisto.fi/en-
433 US/Maps_and_statistics/Air_pollutant_emissions](http://ymparisto.fi/en-US/Maps_and_statistics/Air_pollutant_emissions)). These sources are indeed the most significant
434 sources of NO_x globally (Meixner and Yang, 2006). NO_x, definitive proxy of anthropogenic influence
435 shows a poor correlation with SA ($r_s=0.28$, Fig. 4e) during June-July which could suggest
436 insignificant effect of traffic on the SA concentrations. Unfortunately, the NO_x data from August was
437 unavailable due to instrument malfunction so we cannot provide any correlations for this month.

438 The data presented in Figure 3, where we observe high SA concentrations even when the air mass
439 was marine and the good correlations of SA-MSA (inclusive of insignificant correlations of SA-NO_x)
440 (Fig. 4) indicate towards a greater possibility of the influence of biogenic emissions on the
441 concentrations of SA as compared to the anthropogenic emissions.

442

443 **3.3 Types of nucleation events during the study**

444 During, 25 June 2019–19 August 2019, we observe a number of NPF events characterized by a short
445 appearance of ultrafine particles in the number size distribution lasting for less than one hour. These
446 so-called bursts /spikes appearing at small sizes (sub-3 nm) are indicative of local clustering processes
447 in contrast to regional events, where it is possible to follow the growing particle mode for several

448 hours (Dada et al., 2018; Dal Maso et al., 2005). Local clustering here means that the molecules could
 449 be transported from elsewhere but the actual clustering could have taken place near the experimental
 450 site, indicated by a small bump of clusters (with absolutely little or no growth) as seen in the NAIS
 451 spectra. We do observe transported events (events with a growing particle mode, but no small
 452 particles forming at the site) and non-events days but they are not included in the analysis. This section
 453 discusses the occurrence of local and regional new particle formation events with the focus on: 1)
 454 trace gases variability during the event days, 2) the evolution of different sized particles during these
 455 events, 3) the impact of meteorological parameters and 4) the effect of cyanobacterial bloom on the
 456 events.

457

458 Table 1: Timing and maximum concentration of SA, MSA and IA during local and burst/spike
 459 nucleation events during the study period

Dates	Type of Event	time of NPF (UTC+02:00 h)	SA (max) molec. cm ⁻³	MSA (max) molec. cm ⁻³	IA(max) molec. cm ⁻³
30.06.2019	Regional/ local	8:45-13:23 14:00-16:30	7.9×10^6	5.6×10^5	2.3×10^6
30.07.2019	Regional/ local	7:45 -11:16	1.2×10^7	1.2×10^6	5.3×10^6
11.08.2019	Ion Burst (Spike)	13:40-14:32	1.0×10^7	1×10^6	3.2×10^7
14.08.2019	Ion Burst (Spikes)	8:00-8:20	4.2×10^6	5.3×10^5	8.5×10^6
15.08.2019	Multiple Ion Bursts (Spikes)	6:00, 8:58, 14:00-16:00	6.4×10^6 6.3×10^6 7.0×10^6	5.8×10^5 4.6×10^5 6.8×10^5	2.5×10^6 3.1×10^6 1.5×10^6

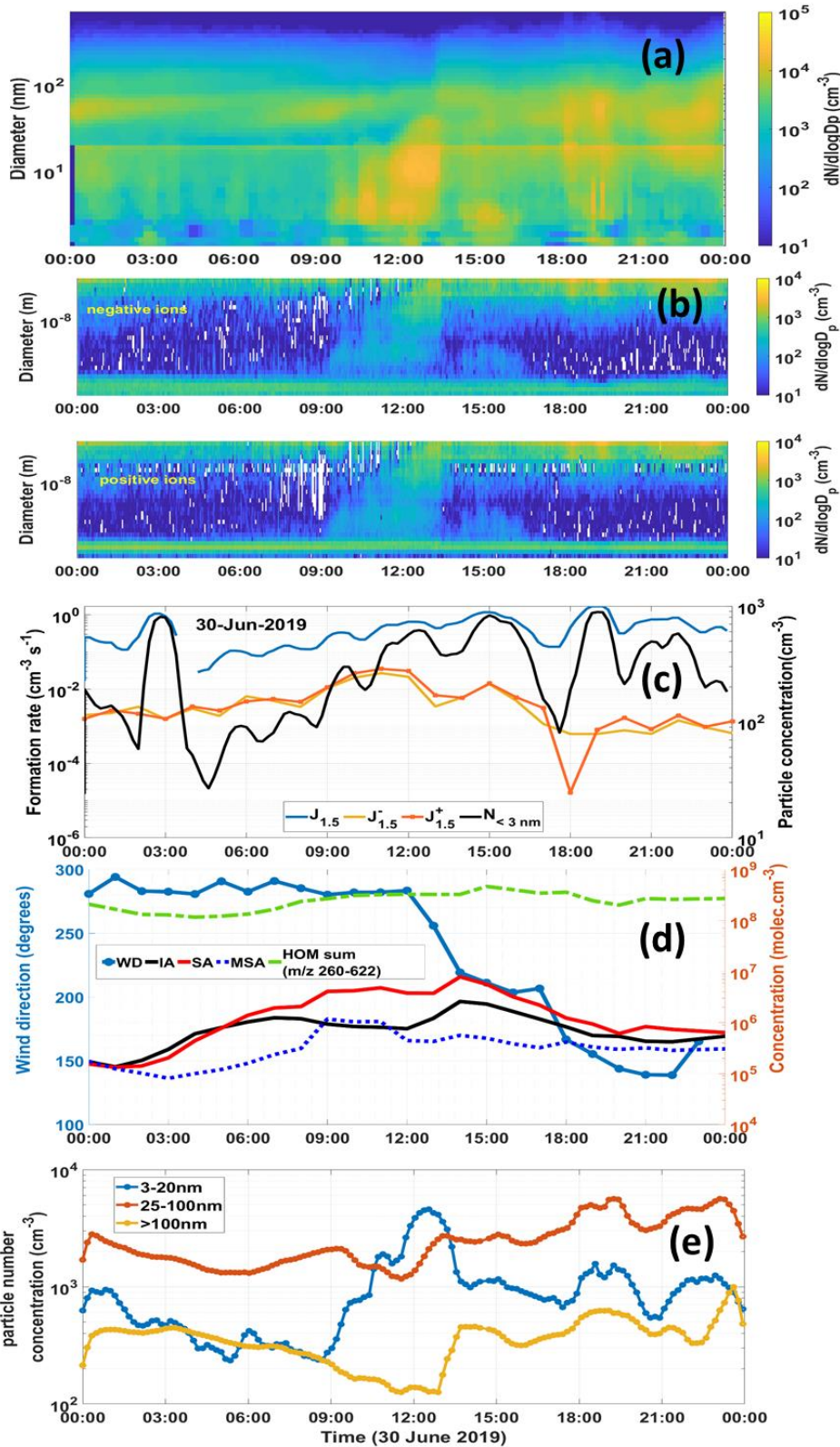
460

461 3.3.1 Nucleation: Regional and Local events

462 A regional NPF event was observed on 30 June 2019, which starts at 08:45 h and ends at 13:23 h (Fig
 463 5a). The negative ion clusters start to increase in concentration first at 08:45 h (Fig. 5b) concurrent
 464 with the increase in concentration of the smallest particles (<3nm) from 10^2 to 10^3 cm⁻³ (Fig. 5c).
 465 Preceding the NPF event the SA concentrations were steadily increasing and subsequently at 09:00
 466 h, SA concentration doubles from 2×10^6 to 4×10^6 molec. cm⁻³ (Fig. 5d), while the particle formation

467 rate at 1.5 nm ($J_{1.5}$) increasing from $0.3 \text{ cm}^{-3} \text{ s}^{-1}$ to $0.6 \text{ cm}^{-3} \text{ s}^{-1}$. $J_{1.5}$ was much higher than either of
468 $J_{+1.5}$ and $J_{-1.5}$, thus indicating a neutral formation pathway rather than ion mediated. Further we also
469 observe local clustering event at 15:00 h with simultaneous increase of concentration of SA and
470 HOMs along with increase in the smallest particle concentration. This possibly indicates the role of
471 SA and HOMs in the nucleation initiation. The high normalized signals of DMA-SA cluster seen
472 during the entire event (increasing from the start of NPF event) possibly indicates that SA clusters
473 initiate the event (Fig. S4a). DMA inclusive of other main methylamines like mono and tri
474 methylamines (Bergman et al., 2015) in the global inventory (Schade and Crutzen, 1995) is
475 contributed through the animal husbandry and other agricultural practices, biomass burning and some
476 contributions from marine and terrestrial sources. Although among these methylamine emissions,
477 generally the trimethylamine dominates (Schade and Crutzen, 1995). Although no estimates of DMA
478 measurements are available from Helsinki region, the DMA in a boreal forest site in Finland has been
479 estimated to be below $\sim 150 \text{ ppqV}$ (Sipilä et al., 2015), measured through a NO_3 -CIMS. Their work
480 also stated that DMA was unlikely the playing an important role in the nucleation process observed
481 at the site.

482 The increase of HOMs is also clearly observed during the event Fig. S4b. Therefore we
483 suggest that nucleation and growth of particles was possibly due to SA-organics which ensures that
484 particles reach the CCN and thus climate relevant diameters. The work of Okuljar et al. (2021) also
485 report an increase in sub-3 nm particles with a simultaneous increase in SA concentration at the
486 SMEAR III site, supporting our observations. However, the role of HOMs in nucleation initiation has
487 not been explored at this site.

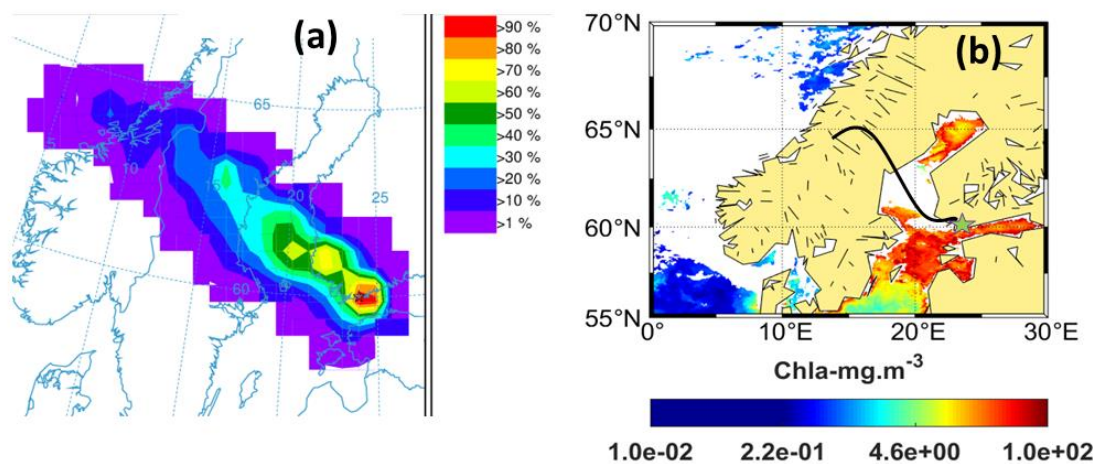


488

489

490 **Figure 5:** NPF Event (Regional and local events), 30 June 2019. (a) Number size distribution of
 491 particles (data from PSM, NAIS and DMPS; size range: sub-3–100nm). (b) Charged particles number
 492 size distribution (negative: upper, positive: lower) obtained from the NAIS. (c) Diurnal variation of

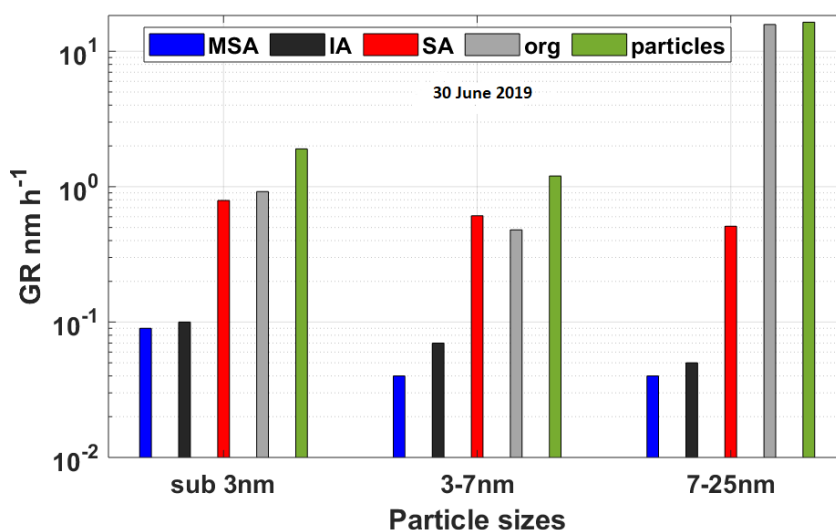
493 formation rates ($J_{1.5}$) of 1.5 nm particles and ions ($J_{1.5}$ and $J^{+}_{1.5}$) on the left axis and particle number
 494 concentrations (1.5–3 nm) on the right axis. (d) Diurnal variation of HOMs SA, IA and MSA with
 495 wind direction (WD). (e) The diurnal variation of particle concentration in nucleation:3–20 nm;
 496 aitken: 25–100 nm and accumulation: >100nm) mode particles during the event (Data from DMPS).



497
 498
 499 **Figure 6:** (a) Trajectory frequency plot (100 a.g.l, arrival time of trajectories at the measurement site:
 500 20:00 h) for 24 h back trajectory using GDAS meteorological input data (frequency grid resolution:
 501 $1.0^\circ \times 1.0^\circ$) (b) Chl-*a* concentrations (GlobColour level-3); Black line shows the trajectory direction and the star point denotes the measurement site .

503
 504 A clear increase in nucleation mode particles is seen during the event, starting at 08:45 h (234 cm^{-3})
 505 and reaching its maximum at 12:30 h (4589 cm^{-3}). This increase in concentration of the nucleation
 506 mode particles was followed by the increase in concentration of Aitken mode and accumulation mode
 507 particles and continues for a couple of hours, indicating growth of particles (Fig. 5e), possibly
 508 reaching to CCN relevant sizes. However, we also observe a drop in Aitken particles before NPF
 509 which also continues during NPF. We speculate it could be due to the change in wind direction
 510 (Väkevä et al., 2000) before NPF. The wind direction relatively remains constant throughout the NPF
 511 so the low concentration of Aitken mode continues. Wind direction changes abruptly at 12:00h and
 512 the Aitken mode particle concentrations increases soon after this change of wind direction (Fig. 5d).
 513 This shows the particles must be the process of growth mostly elsewhere, which is not evident in the
 514 changed air mass, however we still observe almost the same (or even slightly higher) precursor vapor
 515 concentrations, since the wind still passed over the bloom areas before entering our study site.. After
 516 the change in local wind direction, the observed SA and IA slightly increase, and we still observe
 517 clustering (formation of small ions and particles), but no continuous growth typical for regional

518 events. Figure 6a shows that >40% of the trajectories passes above the Swedish island of Gotland
 519 towards southern part of Bothnian Sea. The satellite data shows that the bloom was present in the
 520 Bothnian Sea, but not quite dense as compared to the southern Baltic Sea (south of Gotland island)
 521 and the northern part of the Gulf of Finland (Fig. 6b). The majority of the trajectories did not pass
 522 over the dense cyanobacterial bloom patch during this day (Fig. 6b). The calculated normalized
 523 residence time was higher over the neighboring cities of Helsinki (Southwestern side) and parts of
 524 Bothnian Sea during the event time (see Fig. S3). Thus the land based anthropogenic activities and
 525 biogenic sources both can be contributing to SA concentrations for this event; here we cannot exactly
 526 quantify the source types for SA. However, the source of SA from the local sources such as vehicular
 527 traffic around our measurement site is small (as discussed above) but cannot be completely ignored
 528 (Olin et al., 2020).



529
 530 **Figure 7:** Particle growth rates calculated from the kinetic condensation of gases (data from CI-APi-
 531 ToF) and the measured particle GRs (data from NAIS) in different size classes on 30 June 2019.

532
 533 The particle GR (7–25 nm) for this event was 16.5 nm h^{-1} , which is typical of a coastal
 534 site. Even when several condensing vapors participate in the growth process, growth rates typically
 535 do not exceed 20 nm h^{-1} (Kulmala et al., 2004). The GR for organics was calculated after subtracting
 536 the combined contribution of the GR of SA, IA and MSA from the measured particle GR (Fig. 7).
 537 The GR for organics should be treated as an estimation since no separate GR calculations and
 538 assumptions were used. The calculated growth rates (GR) shows that SA can explain maximum 41%
 539 of the growth of sub-3 nm particles, while IA and MSA can explain only <1% of the GR in this size
 540 range. The GR by SA in the bigger size fraction (7–25 nm) was only 0.51 nm h^{-1} explaining only 3%
 541 of the measured growth rate of particles. This means that vapors other than SA, IA and MSA were

542 responsible for 96% of the measured particle growth. These other vapors could include different
543 organics since organics are known to contribute to growth of particles (Kulmala et al., 1998, 2004;
544 Riipinen et al., 2012; Zheng et al., 2020) and explain particle growth in the boreal forest (Ehn et al.,
545 2014).

546 Another example of regional event (neutral nucleation) probably driven by SA and organics was
547 observed on 30 July 2019 (Fig. S5) which lasts for around four hours. The trajectory frequency plots
548 showed that most of the trajectories were from the northern land areas (including urban cities and
549 boreal forests) of Finland with highest residence times over these land regions (Fig. S6 and S7). Since,
550 the precursor gases from the biogenic origin, IA and MSA, do not show a significant concentration
551 increase as compared to SA, at the start of the event, their contribution towards the initiation of the
552 NPF event may not be as significant as SA. The greater residence times over the land areas clearly
553 support the high SA and organic concentrations seen during the event indicating a SA driven event –
554 with a possible contribution of HOMs (Fig. S7). In this case, SA explains 60% of growth of sub-3nm
555 particles compared to 41% when the dominating trajectories passed over the Gulf of Finland (Fig. 5,
556 30 June 2019). Still, as for the previous case, a major fraction of the growth in the 3–7 nm range
557 remains unexplained by the available acids (SA, IA, MSA) and is expected to be related to the
558 contribution of organics. The GRs explained by SA in both sub-3 nm (1.93 nm h^{-1}) and 3–7 nm (1.46
559 nm h^{-1}) size ranges are 58-59% higher than on 30 June 2019 (0.79 nm h^{-1} and 0.61 nm h^{-1} for sub-3
560 nm and 3–7 nm, respectively) which could be explained by the increase in SA by 52% on 30 July
561 2019. Thus, the events on 30 June and 30 July possibly occur via the nucleation of SA (possibly
562 stabilized by bases eg. ammonia or amines) and the HOMs contribute to growth of particles and
563 possibly in nucleation as well.

564

565 **3.3.2 Nucleation: Burst events**

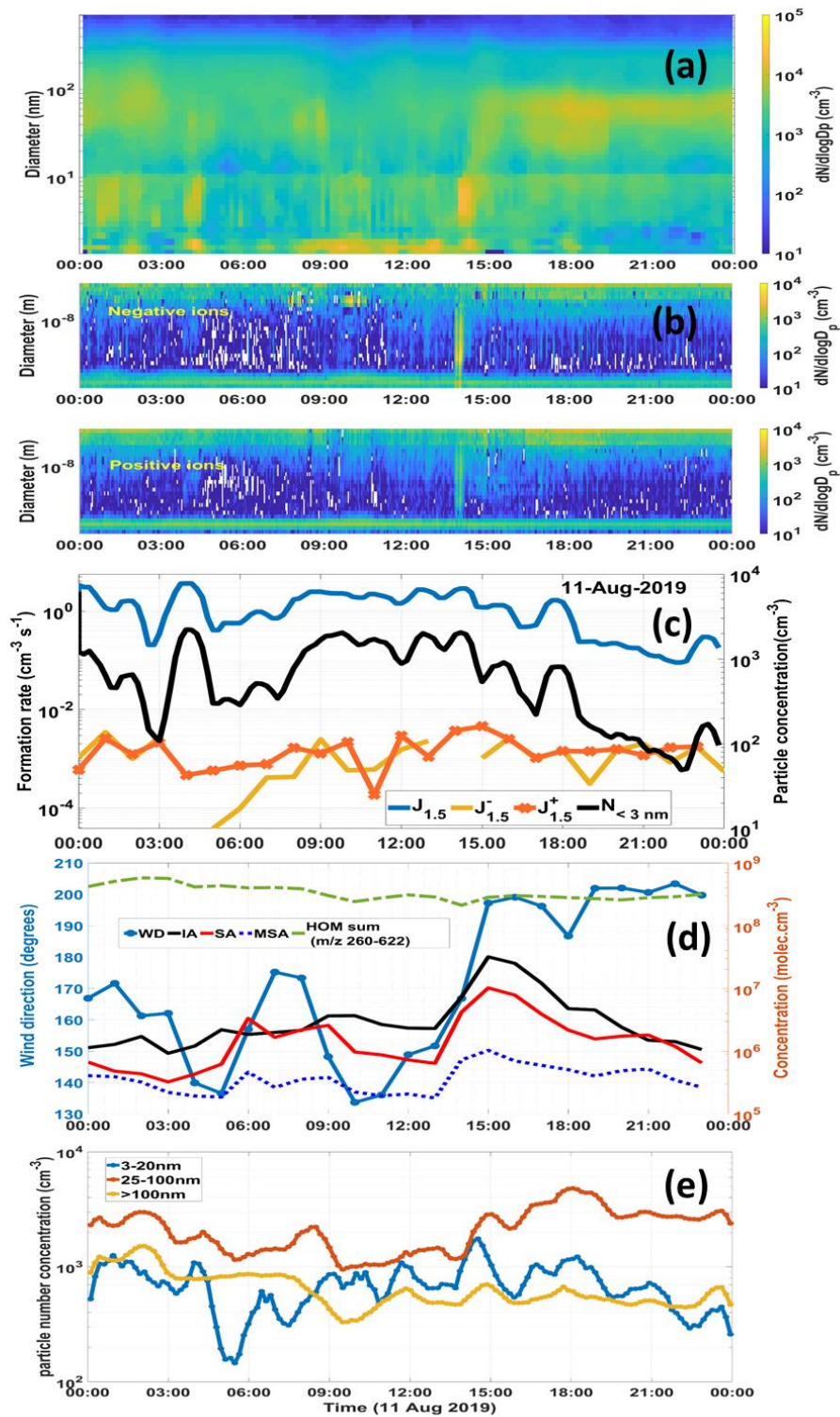
566 **Case 1: Biogenic IA nucleation- burst/spike events, 11 August.2019**

567 Intense burst events are frequently observed at coastal sites accompanied with high concentrations of
568 IA (O'Dowd et al., 2002; Rong et al., 2020; Sipilä et al., 2016). Two of such bursts or spike events
569 were observed on 11 August 2019 at 04:00 h and 13:00 h (Fig. 8a). Only the second spike event was
570 observed in the NAIS size distribution with a higher intensity in the negative mode at 13:00 h (Fig.
571 8b). During both these spike events we observe the formation of clusters (1.5 nm) and the formation
572 rate ($J_{1.5}$) increases from 0.2 to $3.7 \text{ cm}^{-3}\text{s}^{-1}$ during the event with a simultaneous significant increase
573 in the sub-3 nm particle concentrations from ~ 100 to $>2000 \text{ cm}^{-3}$ (Fig. 8c). $J_{1.5}^+$ and $J_{1.5}^-$ remain lower
574 than the total formation rate indicating this event to be a case of neutral nucleation. At the same time,
575 IA shows increase in concentration from $9 \times 10^5 \text{ molec. cm}^{-3}$ at 03:00 h to $1 \times 10^6 \text{ molec. cm}^{-3}$ at 04:00

576 h. During this event the air masses changes from 160° to 140° i.e the direction of the airmass is
577 changed to the Gulf of Finland. In the second burst (at 13:00 h), the IA concentration increases from
578 2×10^6 to 7×10^6 molec. cm^{-3} from 13:00 h to 14:00 h (Fig. 8d) with a slight change in wind direction
579 from 151° to 166° Most of these air masses are from the Gulf of Finland. SA concentration also
580 increased but remained lower than IA during both the burst/spike events indicating a possibility that
581 iodine oxoacid formation initiates cluster formation (He et al., 2021). We observe a growth of
582 particles until 15:00 h in the particle modes (NAIS data, Fig. 7b). However the particles are seen
583 reaching sizes up to size 100 nm (DMPS data , Fig. 8a). The organics almost remain constant within
584 the range of $2\text{--}3 \times 10^8$ molec. cm^{-3} . A further increase in IA concentration, 3×10^7 molec. cm^{-3} occurs
585 at 15:00 h, and the concentration remains in the range of 10^7 molec. cm^{-3} for another two hours (Fig.
586 8d). This was the highest observed IA concentration in the entire measurement period. A recent study
587 by He et al., 2021, indicate that IA concentrations above 1×10^7 molec. cm^{-3} leads to rapid new
588 particle formation at $+10^\circ$ C. At such concentrations the efficacy of iodine oxoacids to form new
589 particles exceeds that of the $\text{H}_2\text{SO}_4\text{-NH}_3$ system at the same acid concentrations. Thus, the
590 concentration of IA found in this event (two times higher than SA during the start of the event), the
591 high formation rates ($>1 \text{ cm}^{-3} \text{ s}^{-1}$) and an unchanged concentration of SA during the event, as
592 compared to the event on 30 June 2019, strongly suggests that it could be an IA driven-NPF event..
593 In addition, a clear increase in the normalized signal of deprotonated IO_3^- with no significant increase
594 in DMA-SA cluster during the event at 13:00 h (Fig. S8a). However, $\text{HNO}_3\text{-IO}_3^-$ cluster was the most
595 abundant followed by the $\text{H}_2\text{O-IO}_3^-$ cluster indicating this event to be IA-driven nucleation. Further,
596 between 14:00–15:00 h, when we observe the highest IA concentrations a subsequent growth of
597 particles is noted. We also observe an increasing number concentration of nucleation mode particles
598 from 13:40 h ($\sim 650 \text{ cm}^{-3}$) to 14:40 h ($\sim 1800 \text{ cm}^{-3}$). After this one hour of intense clustering, the Aitken
599 mode particles also begin to increase in concentration from $\sim 1300 \text{ cm}^{-3}$ to $\sim 4800 \text{ cm}^{-3}$ during 15:00
600 h–18:00 h (Fig. 8e). The total particle concentration increased from $\sim 2400 \text{ cm}^{-3}$ to $\sim 6400 \text{ cm}^{-3}$ within
601 an hour during this burst event. We suggest that this burst event was possibly capable of producing
602 particles big enough to act as CCN. Since it was an intense burst event with no proper horizontal
603 growth (as seen in “banana” type events), we were not able to calculate the growth rate for this
604 particular event. Therefore we are unable to quantify the contribution of IA towards the growth of
605 particles reaching CCN sizes.

606

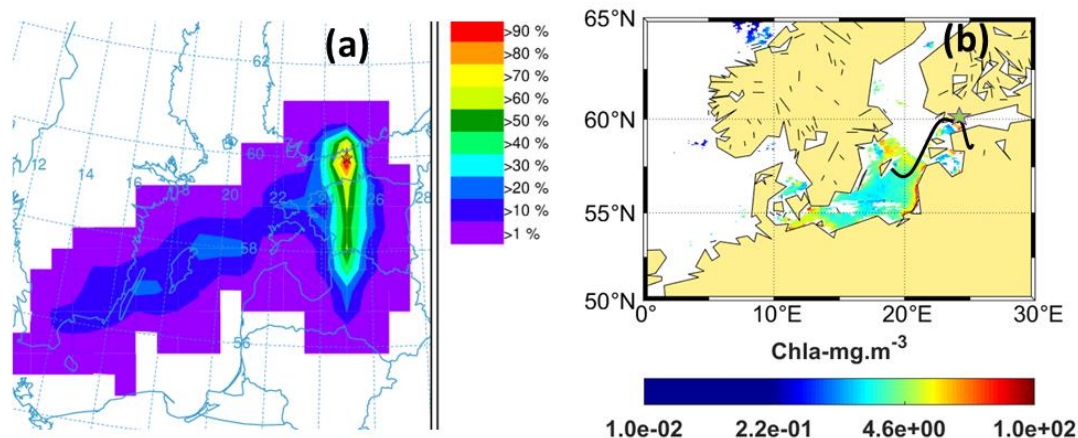
607



608

609 **Figure 8:** Burst/Event, 11 August 2019. (a) Number size distribution of particles (data from PSM,
 610 NAIS and DMPS; size range: 1–100 nm). (b) Charged particles number size distribution (negative:
 611 upper, positive: lower) obtained from the NAIS. (c) Diurnal variation of formation rates ($J_{1.5}$) of 1.5
 612 nm particles and ions ($J_{1.5}^-$ and $J_{1.5}^+$) and total number concentrations of particles (<3 nm, PSM). (d)
 613 Diurnal variation of HOMs, SA, IA and MSA with wind direction (WD). (e) The diurnal variation of

614 particle concentration in nucleation (3–20 nm), Aitken (25–100 nm) and accumulation mode (>100
615 nm) particles (DMPS data).



616

617

618 **Figure: 9** (a) Trajectory frequency plot (100 a.g.l, arrival time of trajectories at measurement site:
619 22:00 h) for 24 hour back trajectory using GDAS meteorological input data (frequency grid
620 resolution: $1.0^{\circ} \times 1.0^{\circ}$) (b) Chl-*a* concentrations (GlobColour level-3); Black line shows the trajectory
621 direction and the star point denotes the measurement site.

622

623 The global radiation and brightness parameter suggest that 11 August 2019 was an
624 overall a cloudy day until 12:30 h (Fig. S9). The weather starts to turn into clear-sky after 13:00 h
625 when the brightness parameter increases from <0.3 to ~0.7 (Fig. S9). Impact of brightness parameter
626 on NPF is also observed in a previous study (Dada et al. 2017). The clearing of the sky could explain
627 the intense spike at 13:00 h in the particle number size distribution as well as in the acid
628 concentrations. For this particular case, we investigated further the source of such high IA
629 concentrations and we found that during this day, the cyanobacterial bloom was observed in three
630 intense patches in the central Baltic sea, southern Gulf of Finland (ship transect route between
631 Helsinki and Tallinn) and Gulf of Riga (Fig. 9b). The trajectory frequency analysis clearly shows that
632 the maximum frequency of trajectories was observed over southern Gulf of Finland (inclusive of the
633 coastal waters of Suomenlinna island) however we do see the air masses coming in from the central
634 Baltic sea as well which was characterized by intense bloom during this day (Fig. 9a). The sea level
635 was also low as it was observed to be 0.8–0.9 m in the coastal waters in around the measurement site
636 (Suomenlinna and Gulf of Finland coastal measurements sites), supporting the exposure of the macro
637 to sunlight which can be a good source of iodine precursors.

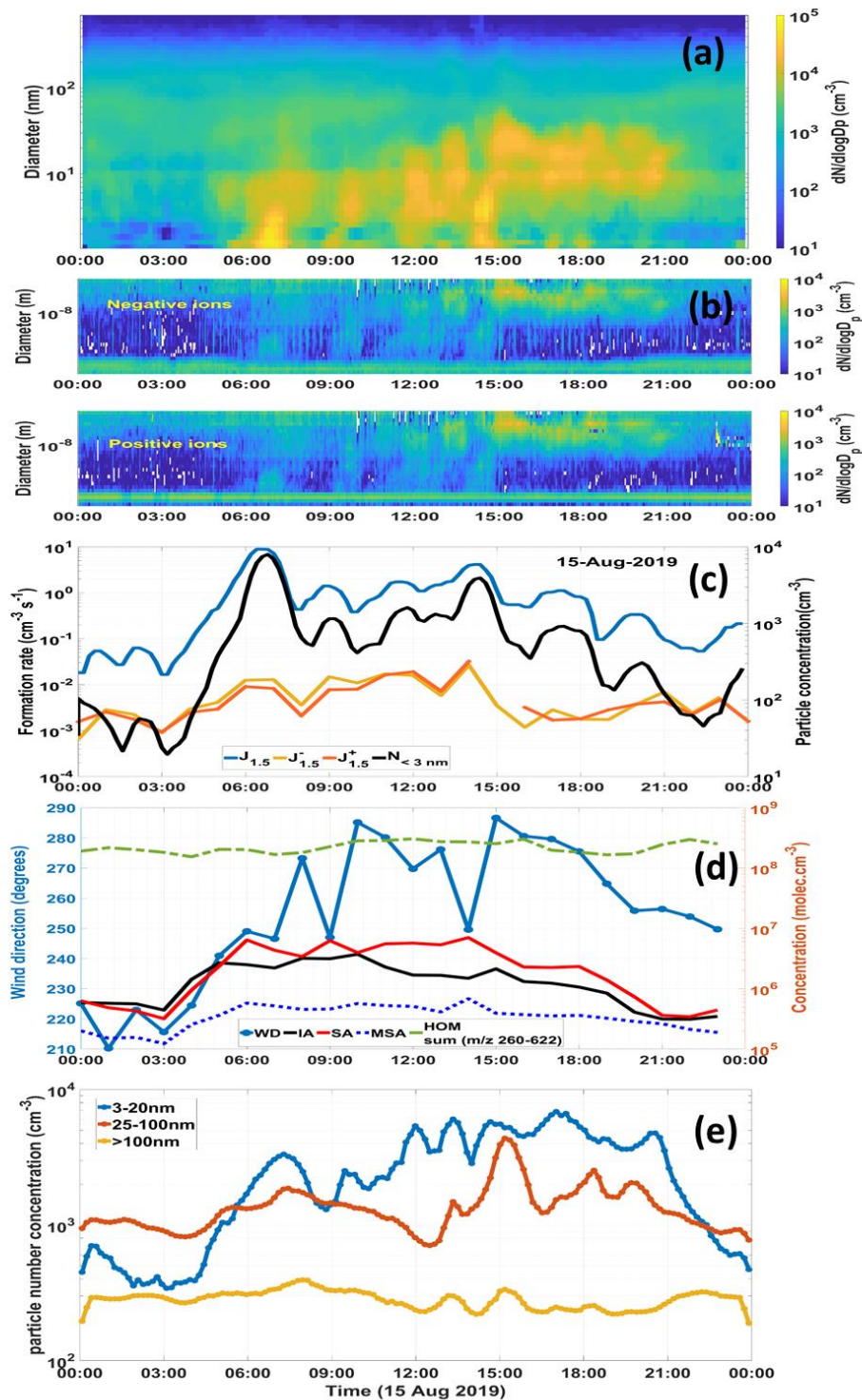
638 The residence time of the airmasses coming from the Gulf of Finland and Northern
639 Baltic Sea were longer than the residence time of the airmasses coming from the neighboring land
640 areas (Fig. S10) clearly explaining the source of high IA observed during the event, which is through
641 the blooms. Further, the airmass was completely marine at 15:00 h when the highest IA is recorded
642 supportive of the marine biogenic source of IA and its transport to the measurement site. The distance
643 from the Gulf of Finland to the measurement site is approximately 5-10 km. With the wind speed of
644 5 m s^{-1} recorded during the event, it takes less than one hour for the emission to transfer to our
645 measurement site. By the time the air mass reached our measurement site from the emission source,
646 a fraction of the emitted I_2 could have oxidized to IA. However, at this point we cannot differentiate
647 between the sources of IA from neighboring coastal waters and the central Baltic Sea but can
648 speculate that most of the IA observed could be sourced from the nearest coastal locations of Gulf of
649 Finland.

650 Another burst/spike event driven by IA occurred on 14 August 2019 (Fig. S11) when
651 the IA concentration was found to be $8 \times 10^6 \text{ molec.cm}^{-3}$ which was 2 times higher than SA
652 concentration ($4 \times 10^6 \text{ molec.cm}^{-3}$). The event did not last more than 30 minutes. The precursor vapor
653 concentration was not large enough for the event to continue or the particles to grow further. The
654 meteorological conditions were very much similar to this event (11 August 2019). For this event also,
655 the airmass was marine with maximum residence times over the Gulf of Finland and Baltic Sea
656 regions. Vicinity of the emissions to the measurement site enabled the detection of these fast-forming
657 clusters.

658 **Case 2: Biogenic SA nucleation –multiple bursts events**

659 Another kind of event was observed on 15 August 2019 (Fig. 10a) where multiple particle bursts are
660 observed and the particles grow to sizes $> 50 \text{ nm}$.

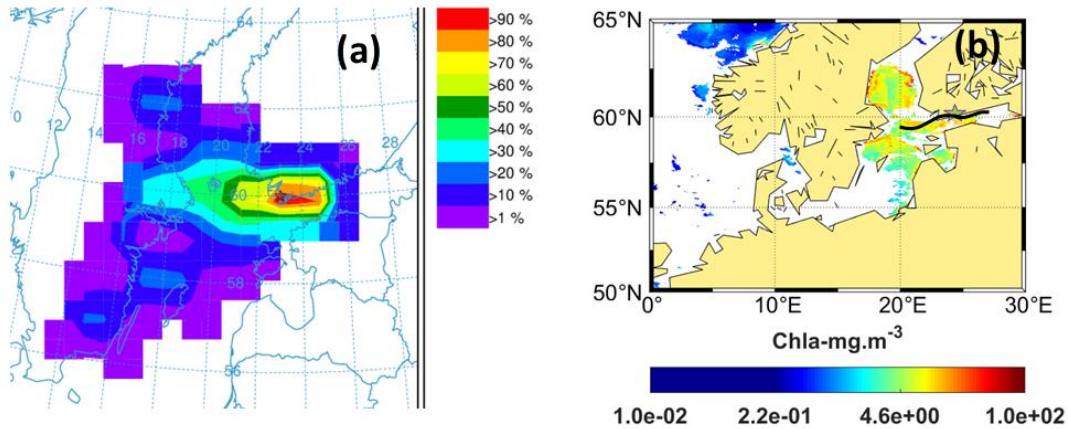
661



662

663 **Figure 10:** Multiple Burst/Spikes, 15 August 2019. (a) Number size distribution of particles (data
 664 from PSM, NAIS and DMPS; size range: 1–100nm). (b) Charged particles number size distribution
 665 (negative: upper, positive: lower) obtained from the NAIS. (c) Diurnal variation of formation rates
 666 ($J_{1.5}$) of 1.5 nm particles and ions ($J_{1.5}^-$ and $J_{1.5}^+$) and total number concentrations of particles (<3 nm,
 667 PSM). (d) Diurnal variation of HOMs SA, IA and MSA with wind direction (WD). (e) The diurnal

668 variation of particle concentration in nucleation (3–20 nm), Aitken (25–100 nm) and accumulation
669 mode (>100 nm) particles (DMPS data).



670

671

672 **Figure 11:** (a) Trajectory frequency plot (100 a.g.l, arrival time of trajectories at the measurement
673 site: 22:00 h) for 24 h back trajectory using GDAS meteorological input data (frequency grid
674 resolution: $1.0^\circ \times 1.0^\circ$) (b) Chl-*a* concentrations (GlobColour level-3); Black line shows the trajectory
675 direction and the star point denotes the measurement site.

676

677 The formation rates for the smallest clusters for both the polarities were the same ($J_{1.5}^+$ and $J_{1.5}^-$) (Fig.
678 10b and c). This was also a case of neutral nucleation as inferred from the relatively high (as compared
679 to ions) $J_{1.5}$ (neutrals). On 15 August there was a sudden change of wind direction from the 180° –
680 215° (prominent wind direction during 11–14 August) to 280° and a series of bursts is triggered with
681 the intense formation of clusters (<3 nm) at each burst (Fig. 10d). The two most intense burst events)
682 were associated with an increase in SA from 2 to 6×10^6 molec. cm^{-3} at 06:00 h, and 5 to 7×10^6
683 molec. cm^{-3} at 14:00 h (Fig. 10d). A third burst at 09:00 h showed an increase in SA from 3 to 6×10^6
684 molec. cm^{-3} at 09:00 h interestingly with IA_{max} : 3×10^6 molec. cm^{-3} . In all the three bursts a
685 simultaneous increase in IA and MSA from 03:00 h to 12:00 h is observed, but the SA concentration
686 was two to three times higher than IA and four to five times higher than MSA concentrations. The
687 most intensive burst was at 14:00 h (as compared burst to 6:00 h) when the SA was 3 times higher
688 than IA. This burst was associated with a significant increase in Aitken mode particle concentration
689 (from 1490 at 14:00 h to 4300 cm^{-3} at 15:00 h). The increase in accumulation particle concentration
690 was seen just after one hour from the start of the bursts for both events (06:00 h and 14:00 h). However
691 the increase in accumulation mode particle concentration for these two events was not very significant
692 ($\sim 100 \text{cm}^{-3}$) although particles reaching a size more than 80 nm (CCN relevant sizes) was observed.

693 We saw DMA-SA clusters during the event (Fig. S12) which supports the observation that this a SA-
694 driven NPF event.

695 During both these events (in fact, all the smaller burst events observed during this day), the
696 trajectories were originating from Sweden (24 h prior to arrival). However, before entering the
697 measurement site the trajectories passed over the Southern part of Gulf of Bothnia and the trajectory
698 frequency was >70% when the wind passed over the cyanobacterial bloom region (Fig. 11a and b).
699 To confirm our findings we checked a day where there was less intense bloom in the Gulf of Finland
700 and Northern Baltic Sea and the dominant airmass did not pass over the bloom patch in Gulf of
701 Finland (Fig. S13) before entering our experimental site. We did not observe an NPF event on this
702 day, thereby suggesting that the airmasses passing over the bloom patches before arriving at our study
703 site were capable of bringing in biogenic precursor vapors capable of initiating NPF events.

704 705 **3.4 Possible contributions of biogenic emissions to Precursor gaseous vapors**

706 Assuming insignificant anthropogenic SA contribution as discussed in section 3.2, we investigated
707 the other possible sources of SA by evaluating the type of algae present in the water bodies from
708 where the air masses travelled during the events. The marine algae produces
709 dimethylsulfoniopropionate (DMSP), which is capable of forming DMS, which subsequently
710 oxidizes into SA and MSA. While very few cyanobacterial species are capable of producing DMSP
711 (Karsten et al., 1996; Jonkers et al., 1998), and its concentration can vary considerably from one
712 species to another (Keller et al., 1989). Moreover, blooms could be well-mixed with other algal
713 species (ESA report, 2000) which are capable of producing DMSP. A recent experiment identified
714 *Aphanizomenon* as the only cyanobacteria producing DMS (Steinke et al., 2018). The Gulfs of
715 Bothnia and Riga are dominated by the genus *Aphanizomenon* (Kownacka et al., 2020). In addition,
716 the Bothnian Sea and Gulf of Finland were found to be rich in cyanobacterial genera of
717 *Aphanizomenon* along with *Nodularia* and *Dolichospermum* (Kownacka et al., 2020). As per the
718 previous studies which were carried out as part of the Baltic-wide monitoring (Kowancka et al., 2020
719 and the references mentioned therein), bloom composition is fairly consistent for different regions
720 and seasons from year to year, which makes it possible for us to make close estimations of the species
721 present during our study in a particular region (from where the airmass travels and the residence time
722 over a particular region).

723 A recent study also indicated that the abundance of DMS producing cyanobacteria,
724 *Aphanizomenon* has increased in the Bothnian Sea due to decreasing salinity (Olofsson et al., 2020).
725 Moreover, marine waters themselves are a large source of DMS (Kettle and Andreae, 2000)

726 explaining the contribution of biogenic SA in the above-mentioned burst events (15 August 2019).
727 Hence to conclude, the marine regions surrounding the experimental site could be potential sources
728 of biogenic SA. Moreover, high iodine emissions could be expected over the Baltic Sea proper region
729 due to the presence of the macroalgal species which are well established and adapted in the Baltic
730 Sea despite its low salinity (Kautsky and Kautsky, 2000; Schagerström et al., 2014) (high IA on 11
731 August 2019 event day). The rocky shorelines of the northern Baltic Sea provides ample habitat for
732 several species of macroalgae, including *F. vesiculosus* (Kautsky & Kautsky 2000, Torn et al., 2006).
733 Previous studies have documented that certain macroalgae contain high levels of iodine (Ar Gall et
734 al., 2004), of which the kelp *Laminaria digitata* stores the highest amount (Ar Gall et al., 2004;
735 Küpper et al., 1998).

736 However recent chamber experiments comparing different species of brown algae
737 found that emission rate of I₂ was higher in the case of *F. vesiculosus* when compared to other species
738 like *L. digitata* (Huang et al., 2013). This could possibly explain the high IA concentration recorded
739 by the CI-APiTOF when the air mass was coming from the Northern Baltic Sea region (11 August
740 2019 and 14 August 2019). High production of macroalgal species is common along the extensive
741 archipelago coastlines of the northern Baltic Sea, and particularly *F. vesiculosus* is likely to contribute
742 with high emission rates, especially when during peak production times when exposed to low sea-
743 levels and direct sunlight. However, partitioning the influence of macroalgae and other microalgae
744 requires further mechanistic studies. We suggest that marine and coastal regions surrounding the
745 measurement site are capable of producing SA and IA during bloom period, which can initiate NPF.

746

747 **4 Conclusions**

748 We studied the composition, concentrations and sources of precursor vapors forming aerosols in
749 Helsinki, Finland during the summer of 2019. The source of precursor gases responsible for new
750 particle formations were assessed by analyzing the meteorological parameters, situation of
751 cyanobacterial/algal bloom in the Baltic Sea. Our study recorded several regional, local and burst
752 events and we found that they were connected to elevated concentrations of SA and IA. The burst
753 /spike events occurred simultaneously with high intensity cyanobacterial/algal blooms in the Baltic
754 Sea.

755 The study draws the following conclusions. 1) Constantly changing algal conditions in
756 Gulf of Bothnia, Gulf of Finland and Baltic Sea could be a significant source for the emission of
757 iodine precursors and DMS. These gases produced by these emissions further oxidize in the
758 atmosphere to form IA and SA, which can be detected by mass spectrometric methods. Interestingly,
759 during marine air mass intrusion with higher residence time over the algal blooms, the gaseous

760 precursors formed from the biological emissions possibly exceeded the gaseous precursors sourced
761 from anthropogenic emissions at the measurement site. In fact, an overall higher impact of biogenic
762 emissions was noted in this semi-urban site particularly during end of July and mid-August when the
763 bloom intensity decreases and the cyanobacteria/macroalgae start to decay and die (while being
764 exposed to sunlight) and consequently produce more emissions (biogenic SA and IA). 2) Moreover,
765 the meteorological conditions like wind direction and possibly wind speed were identified as the most
766 important parameters influencing the precursor vapor concentration reaching the measurement site
767 and thus determining if NPF occurred. Further we also infer that the wind direction played an
768 important role in determining the particle concentrations at the study site. Our study reports, that
769 when the air mass travelled over the land with higher residence time of the air mass over the urban
770 areas, it was enriched with SA and organics from proximal-local sources leading to the occurrence of
771 regional and local events (30 June 2019 and 30 July 2019). In contrast, when the air mass travelled
772 over the water bodies, with higher residence times over the cyanobacterial blooms, the air mass was
773 enriched with biogenic IA and/or SA initiating a burst/spike event at the measurement site (11, 14,
774 15 August 2019). This observation is comparable to other coastal sites like Mace Head, although the
775 NPF events are much stronger in Mace Head, since the measurement site is just at the coast with
776 intensive low tide-high tide periods. 3) The formation rates of 1.5 nm particle and ions suggest that
777 both IA-driven and SA-driven NPF events were neutral nucleation events. 4) The type of
778 phytoplankton species, intensity of the bloom and distance of the bloom from the experimental site
779 is speculated to play an important role in determining the concentrations of precursor gases and thus
780 influence the duration and type of NPF. The IA driven nucleation occurred when the air mass travelled
781 from over the Baltic Sea region, where the coasts are dominated by several species of macroalgae,
782 including *F. vesiculosus*. The SA rich burst events occurred when air mass travelled over the Gulf of
783 Bothnia which was mainly dominated by the cyanobacteria species *Aphanizomenon*. 5) Burst/spike
784 events, connected to high IA concentrations, likely led to fast growth of particles potentially to CCN
785 sizes. The role of stabilizing the IA clusters by SA and ammonia in a semi-urban coastal place needs
786 to be further explored. The growth rate of particles was not fully explained by the SA, IA and MSA
787 alone, this applies especially for 3–7 nm or larger particles, indicating that organics might be playing
788 a critical role in the growth of particles in this semi-urban location. We have significantly high
789 ambient concentrations of HOMs in this study, although the detailed descriptions is beyond the scope
790 of this work.

791 The role of organics (HOM) in the growth of particles is an active research question.
792 Exploring the sources and characterizing them during a bloom period, when the emission of biogenic
793 volatile organics increase with temperature, is crucial to understand the climate linkages of aerosol

794 formation. In order to resolve these links require more quantitative studies are required, which aims
795 to understand the correlation between the quality and quantity of cyanobacterial blooms and the
796 strength of emissions of aerosol precursors. More systematic studies, partitioning the influence of
797 pelagic cyanobacterial blooms and coastal macroalgae on new particle formations, would need to be
798 undertaken.

799

800 *Data availability*

801 Mass spectrometer and air ion spectrometer data related to this article are available upon request to
802 the corresponding author. Rest of the data are available for download from
803 <https://avaa.tdata.fi/web/smart/smear>.

804 *Supplement*

805 The supplement related to this article is available online at:

806 *Author contributions*

807 RCT and TJ, MS designed the experiment, MS, LB, NS, YJT, TC, YJ, JL, ML were involved in the
808 instrument installations and performed calibrations, RCT, collected, processed, analyzed and
809 interpreted the mass spectrometric data. TC, JS, JL, RCT and ML collected and processed the particle
810 data. RCT, LD and KL interpreted the particle data. LD, LB, LQ and XCH performed the calculations.
811 MS, RCT, TJ and MK conceptualized the idea of connecting marine biology and atmospheric
812 processes. AN improvised the marine biology section of the paper. CX carried out Flexpart analysis.
813 MM contributed to the satellite data procurement and its interpretation. All authors contributed
814 commented on the manuscript and improvised the data interpretation.

815

816 *Acknowledgements*

817 We thank the ACTRIS CiGAS-UHEL calibration center for providing facility for CI-APi-TOF
818 calibration and INAR technical staff for support during the entire experiment. We acknowledge
819 Finnish Meteorological Institute for providing open access to oceanographic data used in this study.
820 Financial support: This work was supported by the European Research Council (ERC) under the
821 European Union's Horizon 2020 research and innovation programme (GASPARCON, grant
822 agreement no. 714621) and by the Finnish Academy (grant agreement no. 334514). We also
823 acknowledge Jane and Aatos Erkkö Foundation, ERC ATM-GTP, Flagship ACCC and Aerosols,
824 clouds and trace gases infrastructure (ACTRIS) for funding support. The authors gratefully
825 acknowledge the NOAA Air Resources Laboratory (ARL) for the provision of the HYSPLIT
826 transport and dispersion model and/or READY website (<https://www.ready.noaa.gov>) used in this
827 publication. We also acknowledge Finnish Meteorological Institute for the provision of the wave

828 height data in used this study through the website <https://en.ilmatieteenlaitos.fi/wave-height>. We
829 humbly acknowledge the useful discussion and data reference obtained from Finnish Environmental
830 Institute.

831

832 **References**

833 Allan, J. D., Williams, P. I., Najera, J., Whitehead, J. D., Flynn, M. J., Taylor, J. W., Liu, D., Darbyshire, E.,
834 Carpenter, L. J., Chance, R., Andrews, S. J., Hackenberg, S. C. and McFiggans, G.: Iodine observed in
835 new particle formation events in the Arctic atmosphere during ACCACIA, *Atmos. Chem. Phys.*, 15(10),
836 5599–5609, doi:10.5194/acp-15-5599-2015, 2015.

837 Almeida, J., Schobesberger, S., Kürten, A., Ortega, I. K., Kupiainen-Määttä, O., Praplan, A. P., Adamov, A.,
838 Amorim, A., Bianchi, F., Breitenlechner, M., David, A., Dommen, J., Donahue, N. M., Downard, A.,
839 Dunne, E., Duplissy, J., Ehrhart, S., Flagan, R. C., Franchin, A., Guida, R., Hakala, J., Hansel, A.,
840 Heinritzi, M., Henschel, H., Jokinen, T., Junninen, H., Kajos, M., Kangasluoma, J., Keskinen, H., Kupc,
841 A., Kurtén, T., Kvashin, A. N., Laaksonen, A., Lehtipalo, K., Leiminger, M., Leppä, J., Loukonen, V.,
842 Makhmutov, V., Mathot, S., McGrath, M. J., Nieminen, T., Olenius, T., Onnela, A., Petäjä, T.,
843 Riccobono, F., Riipinen, I., Rissanen, M., Rondo, L., Ruuskanen, T., Santos, F. D., Sarnela, N.,
844 Schallhart, S., Schnitzhofer, R., Seinfeld, J. H., Simon, M., Sipilä, M., Stozhkov, Y., Stratmann, F.,
845 Tomé, A., Tröstl, J., Tsagkogeorgas, G., Vaattovaara, P., Viisanen, Y., Virtanen, A., Vrtala, A., Wagner,
846 P. E., Weingartner, E., Wex, H., Williamson, C., Wimmer, D., Ye, P., Yli-Juuti, T., Carslaw, K. S.,
847 Kulmala, M., Curtius, J., Baltensperger, U., Worsnop, D. R., Vehkamäki, H. and Kirkby, J.: Molecular
848 understanding of sulphuric acid-amine particle nucleation in the atmosphere, *Nature*, 502(7471), 359–
849 363, doi:10.1038/nature12663, 2013.

850 Andersen, J. H., Carstensen, J., Conley, D. J., Dromph, K., Fleming-Lehtinen, V., Gustafsson, B. G., Josefson,
851 A. B., Norkko, A., Villnäs, A. and Murray, C.: Long-term temporal and spatial trends in eutrophication
852 status of the Baltic Sea, *Biol. Rev.*, doi:10.1111/brv.12221, 2017.

853 Ar Gall, E., Küpper, F. C. and Kloareg, B.: A survey of iodine content in *Laminaria digitata*, *Bot. Mar.*,
854 doi:10.1515/BOT.2004.004, 2004.

855 Artaxo, P., Rizzo, L. V., Brito, J. F., Barbosa, H. M. J., Arana, A., Sena, E. T., Cirino, G. G., Bastos, W.,
856 Martin, S. T. and Andreae, M. O.: Atmospheric aerosols in Amazonia and land use change: From natural
857 biogenic to biomass burning conditions, *Faraday Discuss.*, 165, 203–235, doi:10.1039/c3fd00052d,
858 2013.

859 Attard, K. M., Rodil, I. F., Berg, P., Norkko, J., Norkko, A. and Glud, R. N.: Seasonal metabolism and carbon
860 export potential of a key coastal habitat: The perennial canopy-forming macroalga *Fucus vesiculosus*,
861 *Limnol. Oceanogr.*, doi:10.1002/lno.11026, 2019.

862 Baalbaki, R., Pikridas, M., Jokinen, T., Laurila, T., Dada, L., Bezantakos, S., Ahonen, L., Neitola, K., Maisser,
863 A., Bimenyimana, E., Christodoulou, A., Unga, F., Savvides, C., Lehtipalo, K., Kangasluoma, J.,

864 Biskos, G., Petäjä, T., Kerminen, V. M., Sciare, J. and Kulmala, M.: Towards understanding the
865 characteristics of new particle formation in the Eastern Mediterranean, *Atmos. Chem. Phys.*,
866 doi:10.5194/acp-21-9223-2021, 2021.

867 Baccarini, A., Karlsson, L., Dommen, J., Duplessis, P., Vüllers, J., Brooks, I. M., Saiz-Lopez, A., Salter, M.,
868 Tjernström, M., Baltensperger, U., Zieger, P. and Schmale, J.: Frequent new particle formation over the
869 high Arctic pack ice by enhanced iodine emissions, *Nat. Commun.*, doi:10.1038/s41467-020-18551-0,
870 2020.

871 Bates, T.S., Lamb, B.K., Guenther, A., Dignon, J. and Stoiber, R.E.: Sulfur emissions to the atmosphere from
872 natural sources., *J Atmos Chem.*, 14, 315–337, <https://doi.org/10.1007/BF00115242>, 1992. Beck, L. J.,
873 Sarnela, N., Junninen, H., Hoppe, C. J. M., Garmash, O., Bianchi, F., Riva, M., Rose, C., Peräkylä, O.,
874 Wimmer, D., Kausiala, O., Jokinen, T., Ahonen, L., Mikkilä, J., Hakala, J., He, X. C., Kontkanen, J.,
875 Wolf, K. K. E., Cappelletti, D., Mazzola, M., Traversi, R., Petroselli, C., Viola, A. P., Vitale, V., Lange,
876 R., Massling, A., Nøjgaard, J. K., Krejci, R., Karlsson, L., Zieger, P., Jang, S., Lee, K., Vakkari, V.,
877 Lampilahti, J., Thakur, R. C., Leino, K., Kangasluoma, J., Duplissy, E. M., Siivola, E., Marbouti, M.,
878 Tham, Y. J., Saiz-Lopez, A., Petäjä, T., Ehn, M., Worsnop, D. R., Skov, H., Kulmala, M., Kerminen,
879 V. M. and Sipilä, M.: Differing Mechanisms of New Particle Formation at Two Arctic Sites, *Geophys.*
880 *Res. Lett.*, doi:10.1029/2020GL091334, 2021.

881 Benson, D. R., Young, L. H., Kameel, F. R. and Lee, S. H.: Laboratory-measured nucleation rates of sulfuric
882 acid and water binary homogeneous nucleation from the SO₂ + OH reaction, *Geophys. Res. Lett.*,
883 35(11), 1–6, doi:10.1029/2008GL033387, 2008.

884 Bergman, T., Laaksonen, A., Korhonen, H., Malila, J., Dunne, E. M., Mielonen, T., Lehtinen, K. E. J., Kühn,
885 T., Arola, A. and Kokkola, H.: Geographical and diurnal features of amine-enhanced boundary layer
886 nucleation, *J. Geophys. Res. Atmos.*, 120, 9606–9624, doi:10.1002/2015JD023181, 2015.

887 Berresheim, H., Elste, T., Tremmel, H. G., Allen, A. G., Hansson, H. C., Rosman, K., Dal Maso, M., Mäkelä,
888 J. M., Kulmala, M. and O’Dowd, C. D.: Gas-aerosol relationships of H₂SO₄, MSA, and OH:
889 Observations in the coastal marine boundary layer at Mace Head, Ireland, *J. Geophys. Res. Atmos.*,
890 107(19), 1–12, doi:10.1029/2000JD000229, 2002.

891 Bianchi, F., Tröstl, J., Junninen, H., Frege, C., Henne, S., Hoyle, C. R., Molteni, U., Herrmann, E., Adamov,
892 A., Bukowiecki, N., Chen, X., Duplissy, J., Gysel, M., Hutterli, M., Kangasluoma, J., Kontkanen, J.,
893 Kürten, A., Manninen, H. E., Münch, S., Peräkylä, O., Petäjä, T., Rondo, L., Williamson, C.,
894 Weingartner, E., Curtius, J., Worsnop, D. R., Kulmala, M., Dommen, J. and Baltensperger, U.: New
895 particle formation in the free troposphere: A question of chemistry and timing, *Science* (80-.),
896 352(6289), 1109–1112, doi:10.1126/science.aad5456, 2016.

897 Bianchi, F., Junninen, H., Bigi, A., Sinclair, V. A., Dada, L., Hoyle, C. R., Zha, Q., Yao, L., Ahonen, L. R.,
898 Bonasoni, P., Buenrostro Mazon, S., Hutterli, M., Laj, P., Lehtipalo, K., Kangasluoma, J., Kerminen,
899 V. M., Kontkanen, J., Marinoni, A., Mirme, S., Molteni, U., Petäjä, T., Riva, M., Rose, C., Sellegri, K.,
900 Yan, C., Worsnop, D. R., Kulmala, M., Baltensperger, U. and Dommen, J.: Biogenic particles formed

901 in the Himalaya as an important source of free tropospheric aerosols, *Nat. Geosci.*, doi:10.1038/s41561-
902 020-00661-5, 2020.

903 Bigg, E. K. and Turvey, D. E.: Sources of atmospheric particles over Australia, *Atmos. Environ.*, 12(8), 1643–
904 1655, doi:10.1016/0004-6981(78)90313-X, 1978.

905 Boy, M., Karl, T., Turnipseed, A., Mauldin, R. L., Kosciuch, E., Greenberg, J., Rathbone, J., Smith, J., Held,
906 A., Barsanti, K., Wehner, B., Bauer, S., Wiedensohler, A., Bonn, B., Kulmala, M. and Guenther, A.:
907 New particle formation in the front range of the Colorado Rocky Mountains, *Atmos. Chem. Phys.*, 8(6),
908 1577–1590, doi:10.5194/acp-8-1577-2008, 2008.

909 Buenrostro Mazon, S., Kontkanen, J., Manninen, H. E., Nieminen, T., Kerminen, V. M. and Kulmala, M.: A
910 long-term comparison of nighttime cluster events and daytime ion formation in a boreal forest, *Boreal*
911 *Environ. Res.*, 21(3–4), 242–261, 2016.

912 Cai, R. and Jiang, J.: A new balance formula to estimate new particle formation rate: Reevaluating the effect
913 of coagulation scavenging, *Atmos. Chem. Phys.*, 17(20), 12659–12675, doi:10.5194/acp-17-12659-
914 2017, 2017.

915 Carbone, M. S., Park Williams, A., Ambrose, A. R., Boot, C. M., Bradley, E. S., Dawson, T. E., Schaeffer,
916 S. M., Schimel, J. P. and Still, C. J.: Cloud shading and fog drip influence the metabolism of a coastal
917 pine ecosystem *Global Change Biol.*, 19, 484–97, 2013.

918 Chan, T., Cai, R., Ahonen, L. R., Liu, Y., Zhou, Y., Vanhanen, J., Dada, L., Chao, Y., Liu, Y., Wang, L.,
919 Kulmala, M. and Kangasluoma, J.: Assessment of particle size magnifier inversion methods to obtain
920 the particle size distribution from atmospheric measurements, *Atmos. Meas. Tech.*, 13(9), 4885–4898,
921 doi:10.5194/amt-13-4885-2020, 2020.

922 Chen, D., Wang, W., Li, D. and Wang, W.: Atmospheric implication of synergy in methanesulfonic acid-base
923 trimers: A theoretical investigation, *RSC Adv.*, 10(9), 5173–5182, doi:10.1039/c9ra08760e, 2020.

924 Chen, H., Ezell, M. J., Arquero, K. D., Varner, M. E., Dawson, M. L., Gerber, R. B. and Finlayson-Pitts, B. J.:
925 New particle formation and growth from methanesulfonic acid, trimethylamine and water, *Phys. Chem.*
926 *Chem. Phys.*, 17(20), 13699–13709, doi:10.1039/c5cp00838g, 2015.

927 Chen, H., Varner, M. E., Gerber, R. B. and Finlayson-Pitts, B. J.: Reactions of Methanesulfonic Acid with
928 Amines and Ammonia as a Source of New Particles in Air, *J. Phys. Chem. B*, 120(8), 1526–1536,
929 doi:10.1021/acs.jpcc.5b07433, 2016.

930 Croft, B., Martin, R. V., Richard Leaitch, W., Tunved, P., Breider, T. J., D’Andrea, S. D. and Pierce, J. R.:
931 Processes controlling the annual cycle of Arctic aerosol number and size distributions, *Atmos. Chem.*
932 *Phys.*, 16(6), 3665–3682, doi:10.5194/acp-16-3665-2016, 2016.

933 Dada, L., Paasonen, P., Nieminen, T., Buenrostro Mazon, S., Kontkanen, J., Peräkylä, O., Lehtipalo, K.,
934 Hussein, T., Petäjä, T., Kerminen, V. M., Bäck, J. and Kulmala, M.: Long-term analysis of clear-sky
935 new particle formation events and nonevents in Hyytiälä, *Atmos. Chem. Phys.*, doi:10.5194/acp-17-
936 6227-2017, 2017.

937 Dada, L., Chellapermal, R., Buenrostro Mazon, S., Paasonen, P., Lampilahti, J., E Manninen, H., Junninen,

938 H., Petäjä, T., Kerminen, V. M. and Kulmala, M.: Refined classification and characterization of
939 atmospheric new-particle formation events using air ions, *Atmos. Chem. Phys.*, 18(24), 17883–17893,
940 doi:10.5194/acp-18-17883-2018, 2018.

941 Dada, L., Ylivinkka, I., Baalbaki, R., Li, C., Guo, Y., Yan, C., Yao, L., Sarnela, N., Jokinen, T., Daellenbach,
942 K. R., Yin, R., Deng, C., Chu, B., Nieminen, T., Wang, Y., Lin, Z., Thakur, R. C., Kontkanen, J.,
943 Stolzenburg, D., Sipilä, M., Hussein, T., Paasonen, P., Bianchi, F., Salma, I., Weidinger, T., Pikridas,
944 M., Sciare, J., Jiang, J., Liu, Y., Petäjä, T., Kerminen, V. M. and Kulmala, M.: Sources and sinks driving
945 sulfuric acid concentrations in contrasting environments: Implications on proxy calculations, *Atmos.*
946 *Chem. Phys.*, doi:10.5194/acp-20-11747-2020, 2020.

947 Dal Maso, M., Kulmala, M., Riipinen, I., Wagner, R., Hussein, T., Aalto, P. P. and Lehtinen, K. E. J.:
948 Formation and growth of fresh atmospheric aerosols: Eight years of aerosol size distribution data from
949 SMEAR II, Hyytiälä, Finland, *Boreal Environ. Res.*, 10(5), 323–336, 2005.

950 Deng, C., Fu, Y., Dada, L., Yan, C., Cai, R., Yang, D., Zhou, Y., Yin, R., Lu, Y., Li, X., Qiao, X., Fan, X.,
951 Nie, W., Kontkanen, J., Kangasluoma, J., Chu, B., Ding, A., Kerminen, V. M., Paasonen, P., Worsnop,
952 D. R., Bianchi, F., Liu, Y., Zheng, J., Wang, L., Kulmala, M. and Jiang, J.: Seasonal characteristics of
953 new particle formation and growth in urban Beijing, *Environ. Sci. Technol.*, 54(14), 8547–8557,
954 doi:10.1021/acs.est.0c00808, 2020.

955 Dowd, C. D. O., Lowe, J. A., Smith, M. H., Davison, B., Hewitt, C. N. and Harrison, R. M.: Biogenic sulphur
956 emissions and inferred non-sea-salt-sulphate particularly during Events of new particle formation were
957 Instrumentation and Cruise Summary, *Atlantic*, 102(DII), 1997.

958 Du, W., Dada, L., Zhao, J., Chen, X., Daellenbach, K. R., Xie, C., Wang, W., He, Y., Cai, J., Yao, L., Zhang,
959 Y., Wang, Q., Xu, W., Wang, Y., Tang, G., Cheng, X., Kokkonen, T. V., Zhou, W., Yan, C., Chu, B.,
960 Zha, Q., Hakala, S., Kurppa, M., Järvi, L., Liu, Y., Li, Z., Ge, M., Fu, P., Nie, W., Bianchi, F., Petäjä,
961 T., Paasonen, P., Wang, Z., Worsnop, D. R., Kerminen, V. M., Kulmala, M. and Sun, Y.: A 3D study
962 on the amplification of regional haze and particle growth by local emissions, *npj Clim. Atmos. Sci.*,
963 doi:10.1038/s41612-020-00156-5, 2021.

964 Duplissy, J., Merikanto, J., Franchin, A., Tsagkogeorgas, G., Kangasluoma, J., Wimmer, D., Vuollekoski, H.,
965 Schobesberger, S., Lehtipalo, K., Flagan, R. C., Brus, D., Donahue, N. M., Vehkamäki, H., Almeida, J.,
966 Amorim, A., Barmet, P., Bianchi, F., Breitenlechner, M., Dunne, E. M., Guida, R., Henschel, H.,
967 Junninen, H., Kirkby, J., Kürten, A., Kupc, A., Määttänen, A., Makhmutov, V., Mathot, S., Nieminen,
968 T., Onnela, A., Praplan, A. P., Riccobono, F., Rondo, L., Steiner, G., Tome, A., Walther, H.,
969 Baltensperger, U., Carslaw, K. S., Dommen, J., Hansel, A., Petäjä, T., Sipilä, M., Stratmann, F., Vrtala,
970 A., Wagner, P. E., Worsnop, D. R., Curtius, J. and Kulmala, M.: *Journal of Geophysical Research :
971 Atmospheres*, , 1752–1775, doi:10.1002/2015JD023538.Effect, 2016.

972 Eisele, Fred L; Tanner, D. : Measurement of the gas phase concentration of H₂SO₄ and Methane sulphonic
973 acid and estimates of H₂SO₄ production and Loss in Atmosphere, , 98(93), 9001–9010, 1993.

974 Eisele, F. L., Lovejoy, E. R., Kosciuch, E., Moore, K. F., Mauldin, I. L., Smith, J. N., McMurry, P. H. and

975 Iida, K.: Negative atmospheric ions and their potential role in ion-induced nucleation, *J. Geophys. Res.*
976 *Atmos.*, 111(4), doi:10.1029/2005JD006568, 2006.

977 Ehn, M., Thornton, J. A., Kleist, E., Sipilä, M., Junninen, H., Pullinen, I., Springer, M., Rubach, F.,
978 Tillmann, R., Lee, B., Lopez-Hilfiker, F., Andres, S., Acir, I.-H. H., Rissanen, M., Jokinen, T.,
979 Schobesberger, S., Kangasluoma, J., Kontkanen, J., Nieminen, T., Kurtén, T., Nielsen, L. B.,
980 Jørgensen, S., Kjaergaard, H. G., Canagaratna, M., Maso, M. D., Berndt, T., Petäjä, T., Wahner, A.,
981 Kerminen, V.-M. M., Kulmala, M., Worsnop, D. R., Wildt, J. and Mentel, T. F.: A large source of
982 low-volatility secondary organic aerosol, *Nature*, 506(7489), 476–479, doi:10.1038/nature13032,
983 2014.

984 Emery, N. C., D'Antonio, C. M. and Still, C. J.: Fog and live fuel moisture in coastal California shrublands
985 *Ecosphere*, 9, e02167, <https://doi.org/10.1002/ecs2.2167> ,2018.

986 Fiedler, V., Dal Maso, M., Boy, M., Aufmhoff, H., Hoffmann, J., Schuck, T., Birmili, W., Hanke, M., Uecker,
987 J., Arnold, F. and Kulmala, M.: The contribution of sulphuric acid to atmospheric particle formation and
988 growth: A comparison between boundary layers in Northern and Central Europe, *Atmos. Chem. Phys.*,
989 5(7), 1773–1785, doi:10.5194/acp-5-1773-2005, 2005.

990 Flanagan, R. J., Geever, M. and O'Dowd, C. D.: Direct measurements of new-particle fluxes in the coastal
991 environment, *Environ. Chem.*, 2(4), 256–259, doi:10.1071/EN05069, 2005.

992 Funkey, C. P., Conley, D. J., Reuss, N. S., Humborg, C., Jilbert, T. and Slomp, C. P.: Hypoxia sustains
993 cyanobacteria blooms in the Baltic Sea, *Environ. Sci. Technol.*, doi:10.1021/es404395a, 2014.

994 Glasoe, W. A., Volz, K., Panta, B., Freshour, N., Bachman, R., Hanson, D. R., McMurry, P. H. and Jen, C.:
995 Sulfuric acid nucleation: An experimental study of the effect of seven bases, *J. Geophys. Res.*,
996 doi:10.1002/2014JD022730, 2015.

997 He, X. C., Iyer, S., Sipilä, M., Ylisirniö, A., Peltola, M., Kontkanen,
998 J., Baalbaki, R., Simon, M., Kürten, A., Tham, Y. J., Pesonen, J., Ahonen, L. R., Amanatidis, S.,
999 Amorim, A., Baccharini, A., Beck, L., Bianchi, F., Brilke, S., Chen, D., Chiu, R., Curtius, J., Dada, L.,
1000 Dias, A., Dommen, J., Donahue, N. M., Duplissy, J., El Haddad, I., Finkenzeller, H., Fischer, L.,
1001 Heinritzi, M., Hofbauer, V., Kangasluoma, J., Kim, C., Koenig, T. K., Kubečka, J., Kvashnin, A.,
1002 Lamkaddam, H., Lee, C. P., Leiminger, M., Li, Z., Makhmutov, V., Xiao, M., Marten, R., Nie, W.,
1003 Onnela, A., Partoll, E., Petäjä, T., Salo, V. T., Schuchmann, S., Steiner, G., Stolzenburg, D., Stozhkov,
1004 Y., Tauber, C., Tomé, A., Väisänen, O., Vazquez-Pufleau, M., Volkamer, R., Wagner, A. C., Wang, M.,
1005 Wang, Y., Wimmer, D., Winkler, P. M., Worsnop, D. R., Wu, Y., Yan, C., Ye, Q., Lehtinen, K.,
1006 Nieminen, T., Manninen, H. E., Rissanen, M., Schobesberger, S., Lehtipalo, K., Baltensperger, U.,
1007 Hansel, A., Kerminen, V. M., Flagan, R. C., Kirkby, J., Kurtén, T. and Kulmala, M.: Determination of
1008 the collision rate coefficient between charged iodine acid clusters and iodine acid using the appearance
1009 time method, *Aerosol Sci. Technol.*, doi:10.1080/02786826.2020.1839013, 2021a.

1009 He, X. C., Tham, Y. J., Dada, L., Wang, M., Finkenzeller, H., Stolzenburg, D., Iyer, S., Simon, M., Kürten,
1010 A., Shen, J., Rörup, B., Rissanen, M., Schobesberger, S., Baalbaki, R., Wang, D. S., Koenig, T. K.,
1011 Jokinen, T., Sarnela, N., Beck, L. J., Almeida, J., Amanatidis, S., Amorim, A., Ataei, F., Baccharini, A.,

1012 Bertozzi, B., Bianchi, F., Brilke, S., Caudillo, L., Chen, D., Chiu, R., Chu, B., Dias, A., Ding, A.,
1013 Dommen, J., Duplissy, J., Haddad, I. El, Carracedo, L. G., Granzin, M., Hansel, A., Heinritzi, M.,
1014 Hofbauer, V., Junninen, H., Kangasluoma, J., Kempainen, D., Kim, C., Kong, W., Krechmer, J. E.,
1015 Kvashin, A., Laitinen, T., Lamkaddam, H., Lee, C. P., Lehtipalo, K., Leiminger, M., Li, Z., Makhmutov,
1016 V., Manninen, H. E., Marie, G., Marten, R., Mathot, S., Mauldin, R. L., Mentler, B., Möhler, O., Müller,
1017 T., Nie, W., Onnela, A., Petäjä, T., Pfeifer, J., Philippov, M., Ranjithkumar, A., Saiz-Lopez, A., Salma,
1018 I., Scholz, W., Schuchmann, S., Schulze, B., Steiner, G., Stozhkov, Y., Tauber, C., Tomé, A., Thakur,
1019 R. C., Väisänen, O., Vazquez-Pufleau, M., Wagner, A. C., Wang, Y., Weber, S. K., Winkler, P. M., Wu,
1020 Y., Xiao, M., Yan, C., Ye, Q., Ylisirniö, A., Zauner-Wieczorek, M., Zha, Q., Zhou, P., Flagan, R. C.,
1021 Curtius, J., Baltensperger, U., Kulmala, M., Kerminen, V. M., Kurtén, T., et al.: Role of iodine oxoacids
1022 in atmospheric aerosol nucleation, *Science* (80-.), doi:10.1126/science.abe0298, 2021b.

1023 Hoffmann, E. H., Tilgner, A., Schrödner, R., Bräuer, P., Wolke, R. and Herrmann, H.: An advanced modeling
1024 study on the impacts and atmospheric implications of multiphase dimethyl sulfide chemistry, *Proc. Natl.*
1025 *Acad. Sci. U. S. A.*, doi:10.1073/pnas.1606320113, 2016.

1026 Huang, R.-J., Seitz, K., Buxmann, J., Poehler, D., Hornsby, K. E., Carpenter, L. J., Platt, U. and Hoffmann,
1027 T.: In situ measurements of molecular iodine in the marine boundary layer: the link to macroalgae and
1028 the implications for O₃, IO, OIO and NO_x, *Atmos.*
1029 *Chem. Phys. Discuss.*, 10(1), 361–390, doi:10.5194/acpd-10-361-2010, 2010.

1030 Huang, R. J., Thorenz, U. R., Kundel, M., Venables, D. S., Ceburnis, D., Ho, K. F., Chen, J., Vogel, A. L.,
1031 Küpper, F. C., Smyth, P. P. A., Nitschke, U., Stengel, D. B., Berresheim, H., O’Dowd, C. D. and
1032 Hoffmann, T.: The seaweeds *Fucus vesiculosus* and *Ascophyllum nodosum* are significant contributors
1033 to coastal iodine emissions, *Atmos. Chem. Phys.*, 13(10), 5255–5264, doi:10.5194/acp-13-5255-2013,
1034 2013.

1035 Humborg, C., Geibel, M.C., Sun, X., McCrackin, M., Mörth, C.-M., Stranne, C., Jakobsson, M., Gustafsson,
1036 B., Sokolov, A., Norkko, A. and Norkko, J.: High Emissions of Carbon Dioxide and Methane From the
1037 Coastal Baltic Sea at the End of a Summer Heat Wave. *Front. Mar. Sci.* 6, [https://doi.org/10.3389/
1038 fmars.2019.00493](https://doi.org/10.3389/fmars.2019.00493), 2019.

1039 Iida, K., Stolzenburg, M. R., McMurry, P. H. and Smith, J. N.: Estimating nanoparticle growth rates from size-
1040 dependent charged fractions: Analysis of new particle formation events in Mexico City, *J. Geophys.*
1041 *Res. Atmos.*, 113(5), 1–15, doi:10.1029/2007JD009260, 2008.

1042 Jang, E., Park, K. T., Jun Yoon, Y., Kim, T. W., Hong, S. B., Becagli, S., Traversi, R., Kim, J. and Gim, Y.:
1043 New particle formation events observed at the King Sejong Station, Antarctic Peninsula - Part 2: Link
1044 with the oceanic biological activities, *Atmos. Chem. Phys.*, 19(11), 7595–7608, doi:10.5194/acp-19-
1045 7595-2019, 2019.

1046 Jokinen, T., Sipilä, M., Junninen, H., Ehn, M., Lönn, G., Hakala, J., Petäjä, T., Mauldin, R. L., Kulmala, M.
1047 and Worsnop, D. R.: Atmospheric sulphuric acid and neutral cluster measurements using CI-APi-TOF,
1048 *Atmos. Chem. Phys.*, 12(9), 4117–4125, doi:10.5194/acp-12-4117-2012, 2012.

1049 Jokinen, T., Sipilä, M., Kontkanen, J., Vakkari, V., Tisler, P., Duplissy, E. M., Junninen, H., Kangasluoma, J.,
1050 Manninen, H. E., Petäjä, T., Kulmala, M., Worsnop, D. R., Kirkby, J., Virkkula, A. and Kerminen, V.
1051 M.: Ion-induced sulfuric acid–ammonia nucleation drives particle formation in coastal Antarctica, *Sci.*
1052 *Adv.*, 4(11), 1–7, doi:10.1126/sciadv.aat9744, 2018.

1053 Jokinen, T., Kontkanen, J., Lehtipalo, K. et al. Solar eclipse demonstrating the importance of photochemistry
1054 in new particle formation. *Sci Rep* 7, 45707, <https://doi.org/10.1038/srep45707>, 2017. Junninen, H.,
1055 Ehn, M., Petäjä, T., Luosujärvi, L., Kotiaho, T., Kostianen, R., Rohner, U., Gonin, M., Fuhrer, K.,
1056 Kulmala, M. and Worsnop, D. R.: A high-resolution mass spectrometer to measure atmospheric ion
1057 composition, *Atmos. Meas. Tech. Discuss.*, 3(1), 599–636, doi:10.5194/amtd-3-599-2010, 2010.

1058 Kahru, M. and Elmgren, R.: Multidecadal time series of satellite-detected accumulations of cyanobacteria in
1059 the Baltic Sea, *Biogeosciences*, doi:10.5194/bg-11-3619-2014, 2014.

1060 Kautsky, L. and Kautsky, N.: The Baltic Sea, including Bothnian Sea and Bothnian Bay, *Seas Millenn. - an*
1061 *Environ. Eval. - Vol. 1*, 2000.

1062 Keller, M. D., Bellows, W. K. and Guillard, R. R. L.: Dimethyl Sulfide Production in Marine Phytoplankton.,
1063 1989.

1064 Kettle, A. J. and Andreae, M. O.: Flux of dimethylsulfide from the oceans: A comparison of updated data sets
1065 and flux models, *J. Geophys. Res. Atmos.*, doi:10.1029/2000JD900252, 2000.

1066 Kirkby, J., Curtius, J., Almeida, J., Dunne, E., Duplissy, J., Ehrhart, S., Franchin, A., Gagné, S., Ickes, L.,
1067 Kürten, A., Kupc, A., Metzger, A., Riccobono, F., Rondo, L., Schobesberger, S., Tsagkogeorgas, G.,
1068 Wimmer, D., Amorim, A., Bianchi, F., Breitenlechner, M., David, A., Dommen, J., Downard, A., Ehn,
1069 M., Flagan, R. C., Haider, S., Hansel, A., Hauser, D., Jud, W., Junninen, H., Kreissl, F., Kvashin, A.,
1070 Laaksonen, A., Lehtipalo, K., Lima, J., Lovejoy, E. R., Makhmutov, V., Mathot, S., Mikkilä, J.,
1071 Minginette, P., Mogo, S., Nieminen, T., Onnela, A., Pereira, P., Petäjä, T., Schnitzhofer, R., Seinfeld, J.
1072 H., Sipilä, M., Stozhkov, Y., Stratmann, F., Tomé, A., Vanhanen, J., Viisanen, Y., Vrtala, A., Wagner,
1073 P. E., Walther, H., Weingartner, E., Wex, H., Winkler, P. M., Carslaw, K. S., Worsnop, D. R.,
1074 Baltensperger, U. and Kulmala, M.: Role of sulphuric acid, ammonia and galactic cosmic rays in
1075 atmospheric aerosol nucleation, *Nature*, 476(7361), 429–435, doi:10.1038/nature10343, 2011.

1076 Kirkby, J., Duplissy, J., Sengupta, K., Frege, C., Gordon, H., Williamson, C., Heinritzi, M., Simon, M., Yan,
1077 C., Almeida, J., Trostl, J., Nieminen, T., Ortega, I. K., Wagner, R., Adamov, A., Amorim, A.,
1078 Bernhammer, A. K., Bianchi, F., Breitenlechner, M., Brilke, S., Chen, X., Craven, J., Dias, A., Ehrhart,
1079 S., Flagan, R. C., Franchin, A., Fuchs, C., Guida, R., Hakala, J., Hoyle, C. R., Jokinen, T., Junninen, H.,
1080 Kangasluoma, J., Kim, J., Krapf, M., Kurten, A., Laaksonen, A., Lehtipalo, K., Makhmutov, V., Mathot,
1081 S., Molteni, U., Onnela, A., Perakyla, O., Piel, F., Petaja, T., Praplan, A. P., Pringle, K., Rap, A.,
1082 Richards, N. A. D., Riipinen, I., Rissanen, M. P., Rondo, L., Sarnela, N., Schobesberger, S., Scott, C.
1083 E., Seinfeld, J. H., Sipilä, M., Steiner, G., Stozhkov, Y., Stratmann, F., Tomé, A., Virtanen, A., Vogel,
1084 A. L., Wagner, A. C., Wagner, P. E., Weingartner, E., Wimmer, D., Winkler, P. M., Ye, P., Zhang, X.,
1085 Hansel, A., Dommen, J., Donahue, N. M., Worsnop, D. R., Baltensperger, U., Kulmala, M., Carslaw,

1086 K. S. and Curtius, J.: Ion-induced nucleation of pure biogenic particles, *Nature*, 533(7604), 521–526,
1087 doi:10.1038/nature17953, 2016.

1088 Knutson, E. O. and Whitby, K. T.: Aerosol classification by electric mobility: apparatus, theory, and
1089 applications, *J. Aerosol Sci.*, 6(6), 443–451, doi:10.1016/0021-8502(75)90060-9, 1975.

1090 Knutson, E. O., Whitby, K. T., Fiedler, V., Dal Maso, M., Boy, M., Aufmhoff, H., Hoffmann, J., Schuck, T.,
1091 Birmili, W., Hanke, M., Uecker, J., Arnold, F., Kulmala, M., Petäjä, T., Nieminen, T., Sipilä, M.,
1092 Manninen, H. E., Lehtipalo, K., Dal Maso, M., Aalto, P. P., Junninen, H., Paasonen, P., Riipinen, I.,
1093 Lehtinen, K. E. J., Laaksonen, A., Kerminen, V. M., Croft, B., Martin, R. V., Richard Leitch, W.,
1094 Tunved, P., Breider, T. J., D’Andrea, S. D., Pierce, J. R., Glasoe, W. A., Volz, K., Panta, B., Freshour,
1095 N., Bachman, R., Hanson, D. R., McMurry, P. H., Jen, C., Suikkanen, S., Pulina, S., Engström-Öst, J.,
1096 Lehtiniemi, M., Lehtinen, S., Brutemark, A., Berresheim, H., Elste, T., Tremmel, H. G., Allen, A. G.,
1097 Hansson, H. C., Rosman, K., Dal Maso, M., Mäkelä, J. M., Kulmala, M., O’Dowd, C. D., Lehtinen, K.
1098 E. J., Kulmala, M., Manninen, H. E., Nieminen, T., Asmi, E., Gagné, S., Häkkinen, S., Lehtipalo, K.,
1099 Aalto, P. P., Vana, M., Mirme, A., Mirme, S., Hörrak, U., Plass-Dülmer, C., Stange, G., Kiss, G., Hoffer,
1100 A., Töro, N., Moerman, M., Henzing, B., De Leeuw, G., Brinkenberg, M., Kouvarakis, G. N.,
1101 Bougiatioti, A., Mihalopoulos, N., O’Dowd, C. D., Ceburnis, D., Arneth, A., Svenningsson, B.,
1102 Swietlicki, E., Tarozzi, L., Decesari, S., Facchini, M. C., Birmili, W., Sonntag, A., Wiedensohler, A.,
1103 Boulon, J., Sellegri, K., Laj, P., Gysel, M., Bukowiecki, N., Weingartner, E., et al.: Quantification of the
1104 volatility of secondary organic compounds in ultrafine particles during nucleation events, *Atmos. Chem.*
1105 *Phys.*, 10(4), 1–10, doi:10.1039/c9ra08760e, 2016.

1106 Kownacka, J., Calkiewicz, J. and Kornijów, R.: A turning point in the development of phytoplankton in the
1107 Vistula Lagoon (southern Baltic Sea) at the beginning of the 21st century, *Oceanologia*,
1108 doi:10.1016/j.oceano.2020.08.004, 2020.

1109 Kulmala, M., Toivonen, A., Mäkelä, J. M. and Laaksonen, A.: Analysis of the growth of nucleation mode
1110 particles observed in Boreal forest, *Tellus, Ser. B Chem. Phys. Meteorol.*,
1111 doi:10.3402/tellusb.v50i5.16229, 1998.

1112 Kulmala, M., Laakso, L., Lehtinen, K. E. J., Riipinen, I., Dal Maso, M., Anttila, T., Kerminen, V.-M., Hörrak,
1113 U., Vana, M. and Tammet, H.: Initial steps of aerosol growth, *Atmos. Chem. Phys.*, doi:10.5194/acp-4-
1114 2553-2004, 2004.

1115 Kulmala, M., Petäjä, T., Mönkkönen, P., Koponen, I. K., Dal Maso, M., Aalto, P. P., Lehtinen, K. E. J. and
1116 Kerminen, V. M.: On the growth nucleation mode particles: Source rates of condensable vapor in
1117 polluted and clean environments, *Atmos. Chem. Phys.*, 5(2), 409–416, doi:10.5194/acp-5-409-2005,
1118 2005.

1119 Kulmala, M., Petäjä, T., Nieminen, T., Sipilä, M., Manninen, H. E., Lehtipalo, K., Dal Maso, M., Aalto, P. P.,
1120 Junninen, H., Paasonen, P., Riipinen, I., Lehtinen, K. E. J., Laaksonen, A. and Kerminen, V. M.:
1121 Measurement of the nucleation of atmospheric aerosol particles, *Nat. Protoc.*, 7(9), 1651–1667,
1122 doi:10.1038/nprot.2012.091, 2012.

- 1123 Kulmala, M., Kontkanen, J., Junninen, H., Lehtipalo, K., Manninen, H. E., Nieminen, T., Petäjä, T., Sipilä,
1124 M., Schobesberger, S., Rantala, P., Franchin, A., Jokinen, T., Järvinen, E., Äijälä, M., Kangasluoma, J.,
1125 Hakala, J., Aalto, P. P., Paasonen, P., Mikkilä, J., Vanhanen, J., Aalto, J., Hakola, H., Makkonen, U.,
1126 Ruuskanen, T., Mauldin, R. L., Duplissy, J., Vehkamäki, H., Bäck, J., Kortelainen, A., Riipinen, I.,
1127 Kurtén, T., Johnston, M. V., Smith, J. N., Ehn, M., Mentel, T. F., Lehtinen, K. E. J., Laaksonen, A.,
1128 Kerminen, V. M. and Worsnop, D. R.: Direct observations of atmospheric aerosol nucleation, *Science*
1129 (80), 339(6122), 943–946, doi:10.1126/science.1227385, 2013.
- 1130 Kulmala, M., Petäjä, T., Kerminen, V. M., Kujansuu, J., Ruuskanen, T., Ding, A., Nie, W., Hu, M., Wang, Z.,
1131 Wu, Z., Wang, L. and Worsnop, D. R.: On secondary new particle formation in China, *Front. Environ.*
1132 *Sci. Eng.*, 10(5), 1–10, doi:10.1007/s11783-016-0850-1, 2016.
- 1133 Kulmala, M., Kerminen, V. M., Petäjä, T., Ding, A. J. and Wang, L.: Atmospheric gas-to-particle conversion:
1134 Why NPF events are observed in megacities?, *Faraday Discuss.*, 200, 271–288,
1135 doi:10.1039/c6fd00257a, 2017.
- 1136 Kuosa, H., Fleming-Lehtinen, V., Lehtinen, S., Lehtiniemi, M., Nygård, H., Raateoja, M., Raitaniemi, J.,
1137 Tuimala, J., Uusitalo, L. and Suikkanen, S.: A retrospective view of the development of the Gulf of
1138 Bothnia ecosystem, *J. Mar. Syst.*, 167, 78–92, doi:10.1016/j.jmarsys.2016.11.020, 2017.
- 1139 Küpper, F. C., Schweigert, N., Ar Gall, E., Legendre, J. M., Vilter, H. and Kloareg, B.: Iodine uptake in
1140 Laminariales involves extracellular, haloperoxidase-mediated oxidation of iodide, *Planta*,
1141 doi:10.1007/s004250050469, 1998.Kürten, A., Jokinen, T., Simon, M., Sipilä, M., Sarnela, N.,
1142 Junninen, H., Adamov, A., Almeida, J., Amorim, A., Bianchi, F., Breitenlechner, M., Dommen, J.,
1143 Donahue, N. M., Duplissy, J., Ehrhart, S., Flagan, R. C., Franchin, A., Hakala, J., Hansel, A., Heinritzi,
1144 M., Hutterli, M., Kangasluoma, J., Kirkby, J., Laaksonen, A., Lehtipalo, K., Leiminger, M.,
1145 Makhmutov, V., Mathot, S., Onnela, A., Petäjä, T., Praplan, A. P., Riccobono, F., Rissanen, M. P.,
1146 Rondo, L., Schobesberger, S., Seinfeld, J. H., Steiner, G., Tomé, A., Tröstl, J., Winkler, P. M.,
1147 Williamson, C., Wimmer, D., Ye, P., Baltensperger, U., Carslaw, K. S., Kulmala, M., Worsnop, D. R.
1148 and Curtius, J.: Neutral molecular cluster formation of sulfuric acid-dimethylamine observed in real
1149 time under atmospheric conditions, *Proc. Natl. Acad. Sci. U. S. A.*, 111(42), 15019–15024,
1150 doi:10.1073/pnas.1404853111, 2014.
- 1151 Kürten, A., Münch, S., Rondo, L., Bianchi, F., Duplissy, J., Jokinen, T., Junninen, H., Sarnela, N.,
1152 Schobesberger, S., Simon, M., Sipilä, M., Almeida, J., Amorim, A., Dommen, J., Donahue, N. M.,
1153 Dunne, E. M., Flagan, R. C., Franchin, A., Kirkby, J., Kupc, A., Makhmutov, V., Petäjä, T., Praplan, A.
1154 P., Riccobono, F., Steiner, G., Tomé, A., Tsagkogeorgas, G., Wagner, P. E., Wimmer, D., Baltensperger,
1155 U., Kulmala, M., Worsnop, D. R. and Curtius, J.: Thermodynamics of the formation of sulfuric acid
1156 dimers in the binary (H₂SO₄-H₂O) and ternary (H₂SO₄-H₂O-NH₃) system, *Atmos. Chem. Phys.*,
1157 15(18), 10701–10721, doi:10.5194/acp-15-10701-2015, 2015.
- 1158 Kürten, A., Bianchi, F., Almeida, J., Kupiainen-Määttä, O., Dunne, E. M., Duplissy, J., Williamson, C.,
1159 Barmet, P., Breitenlechner, M., Dommen, J., Donahue, N. M., Flagan, R. C., Franchin, A., Gordon, H.,

1160 Hakala, J., Hansel, A., Heinritzi, M., Ickes, L., Jokinen, T., Kangasluoma, J., Kim, J., Kirkby, J., Kupc,
 1161 A., Lehtipalo, K., Leiminger, M., Makhmutov, V., Onnela, A., Ortega, I. K., Petäjä, T., Praplan, A. P.,
 1162 Riccobono, F., Rissanen, M. P., Rondo, L., Schnitzhofer, R., Schobesberger, S., Smith, J. N., Steiner,
 1163 G., Stozhkov, Y., Tomé, A., Tröstl, J., Tsagkogeorgas, G., Wagner, P. E., Wimmer, D., Ye, P.,
 1164 Baltensperger, U., Carslaw, K., Kulmala, M. and Curtius, J.: Experimental particle formation rates
 1165 spanning tropospheric sulfuric acid and ammonia abundances, ion production rates, and temperatures,
 1166 *J. Geophys. Res.*, doi:10.1002/2015JD023908, 2016.

1167 Kurten, T., Petäjä, T., Smith, J., Ortega, I. K., Sipilä, M., Junninen, H., Ehn, M., Vehkamäki, H., Mauldin,
 1168 L., Worsnop, D. R. and Kulmala, M.: The effect of H₂SO₄ – amine clustering on chemical ionization
 1169 mass spectrometry (CIMS) measurements of gas-phase sulfuric acid, *Atmos. Chem. Phys.*, 11, 3007–
 1170 3019, doi:10.5194/acp-11-3007-2011, 2011.

1171 Kyrö, E. M., Väänänen, R., Kerminen, V. M., Virkkula, A., Petäjä, T., Asmi, A., Dal Maso, M., Nieminen, T.,
 1172 Juhola, S., Shcherbinin, A., Riipinen, I., Lehtipalo, K., Keronen, P., Aalto, P. P., Hari, P. and Kulmala,
 1173 M.: Trends in new particle formation in eastern Lapland, Finland: Effect of decreasing sulfur emissions
 1174 from Kola Peninsula, *Atmos. Chem. Phys.*, 14(9), 4383–4396, doi:10.5194/acp-14-4383-2014, 2014.

1175 Lawson, D. M., Clemesha, R.E.S., Vanderplank, S., Gershunov, A. and Cayan, D.: Impacts and influences of
 1176 coastal low clouds and fog on biodiversity in San Diego California’s Fourth Climate Change
 1177 Assessment CCCA4-EXT-2018-010 69–89, [https://www.energy.ca.gov/sites/default/files/2019-](https://www.energy.ca.gov/sites/default/files/2019-12/Biodiversity_CCCA4-EXT-2018-010_ada_0.pdf)
 1178 [12/Biodiversity_CCCA4-EXT-2018-010_ada_0.pdf](https://www.energy.ca.gov/sites/default/files/2019-12/Biodiversity_CCCA4-EXT-2018-010_ada_0.pdf), 2018.

1179 Lehtipalo, K., Yan, C., Dada, L., Bianchi, F., Xiao, M., Wagner, R., Stolzenburg, D., Ahonen, L. R., Amorim,
 1180 A., Baccarini, A., Bauer, P. S., Baumgartner, B., Bergen, A., Bernhammer, A. K., Breitenlechner, M.,
 1181 Brilke, S., Buchholz, A., Mazon, S. B., Chen, D., Chen, X., Dias, A., Dommen, J., Draper, D. C.,
 1182 Duplissy, J., Ehn, M., Finkenzeller, H., Fischer, L., Frege, C., Fuchs, C., Garmash, O., Gordon, H.,
 1183 Hakala, J., He, X., Heikkinen, L., Heinritzi, M., Helm, J. C., Hofbauer, V., Hoyle, C. R., Jokinen, T.,
 1184 Kangasluoma, J., Kerminen, V.-M., Kim, C., Kirkby, J., Kontkanen, J., Kürten, A., Lawler, M. J., Mai,
 1185 H., Mathot, S., Mauldin III, R. L., Molteni, U., Nichman, L., Nie, W., Nieminen, T., Ojdanic, A., Onnela,
 1186 A., Passananti, M., Petäjä, T., Piel, F., Pospisilova, V., Quéléver, L. L. J., Rissanen, M. P., Rose, C.,
 1187 Sarnela, N., Schallhart, S., Schuchmann, S., Sengupta, K., Simon, M., Sipilä, M., Tauber, C., Tomé,
 1188 A., Tröstl, J., Väisänen, O., Vogel, A. L., Volkamer, R., Wagner, A. C., Wang, M., Weitz, L., Wimmer,
 1189 D., Ye, P., Ylisirniö, A., Zha, Q., Carslaw, K. S., Curtius, J., Donahue, N. M., Flagan, R. C., Hansel, A.,
 1190 Riipinen, I., Virtanen, A., Winkler, P. M., Baltensperger, U., Kulmala, M., and Worsnop, D. R.:
 1191 Multicomponent new particle formation from sulfuric acid, ammonia, and 979 biogenic vapors, *Sci.*
 1192 *Adv.*, 12, doi: 10.1126/sciadv.aau5363, 2018.

1193 Lehtipalo, K., Leppä, J., Kontkanen, J., Kangasluoma, J., Franchin, A., Wimmer, D., Schobesberger, S.,
 1194 Junninen, H., Petäjä, T., Sipilä, M., Mikkilä, J., Vanhanen, J., Worsnop, D. R. and Kulmala, M.:
 1195 Methods for determining particle size distribution and growth rates between 1 and 3 nm using the
 1196 Particle Size Magnifier, *Boreal Environ. Res.*, 19(September), 215–236, 2014.

- 1197 Leino, K., Nieminen, T., Manninen, H. E., Petäjä, T., Kerminen, V. M. and Kulmala, M.: Intermediate ions as
1198 a strong indicator of new particle formation bursts in boreal forest, *Boreal Environ. Res.*, 21(3–4), 274–
1199 286, 2016.
- 1200 Mahajan, A. S., Oetjen, H., Saiz-Lopez, A., Lee, J. D., McFiggans, G. B. and Plane, J. M. C.: Reactive iodine
1201 species in a semi-polluted environment, *Geophys. Res. Lett.*, 36(16), 6–11,
1202 doi:10.1029/2009GL038018, 2009.
- 1203 Mahajan, A. S., Sorribas, M., Martín, J. C. G., MacDonald, S. M., Gil, M., Plane, J. M. C. and Saiz-Lopez, A.:
1204 Concurrent observations of atomic iodine, molecular iodine and ultrafine particles in a coastal
1205 environment, *Atmos. Chem. Phys.*, 11(6), 2545–2555, doi:10.5194/acp-11-2545-2011, 2011.
- 1206 Manninen, H. E., Nieminen, T., Asmi, E., Gagné, S., Häkkinen, S., Lehtipalo, K., Aalto, P., Vana, M., Mirme,
1207 A., Mirme, S., Hörrak, U., Plass-Dülmer, C., Stange, G., Kiss, G., Hoffer, A., Töro, N., Moerman, M.,
1208 Henzing, B., De Leeuw, G., Brinkenberg, M., Kouvarakis, G. N., Bougiatioti, A., Mihalopoulos, N.,
1209 O’Dowd, C., Ceburnis, D., Arneth, A., Svenningsson, B., Swietlicki, E., Tarozzi, L., Decesari, S.,
1210 Facchini, M. C., Birmili, W., Sonntag, A., Wiedensohler, A., Boulon, J., Sellegri, K., Laj, P., Gysel, M.,
1211 Bukowiecki, N., Weingartner, E., Wehrle, G., Laaksonen, A., Hamed, A., Joutsensaari, J., Petäjä, T.,
1212 Kerminen, V. M. and Kulmala, M.: EUCAARI ion spectrometer measurements at 12 European sites-
1213 analysis of new particle formation events, *Atmos. Chem. Phys.*, 10(16), 7907–7927, doi:10.5194/acp-
1214 10-7907-2010, 2010.
- 1215 Mauldin, R. L., Eisele, F. L., Kosciuch, E., Shetter, R., Lefer, B., Buhr, M., Chen, G., Wang, P. and Davis, D.:
1216 Oil] andjO (‘ D), , 28(19), 3629–3632, 2001.
- 1217 McFiggans, G., Coe, H., Burgess, R., Allan, J., Cubison, M., Alfarra, M. R., Saunders, R., Saiz-Lopez, A.,
1218 Plane, J. M. C., Wevill, D. J., Carpenter, L. J., Rickard, A. R. and Monks, P. S.: Direct evidence for
1219 coastal iodine particles from *Laminaria* macroalgae - Linkage to emissions of molecular iodine, *Atmos.*
1220 *Chem. Phys.*, 4(3), 701–713, doi:10.5194/acp-4-701-2004, 2004.
- 1221 McFiggans, G., Bale, C. S. E., Ball, S. M., Beames, J. M., Bloss, W. J., Carpenter, L. J., Dorsey, J., Dunk, R.,
1222 Flynn, M. J., Furneaux, K. L., Gallagher, M. W., Heard, D. E., Hollingsworth, A. M., Hornsby, K.,
1223 Ingham, T., Jones, C. E., Jones, R. L., Kramer, L. J., Langridge, J. M., Leblanc, C., LeCrane, J. P., Lee,
1224 J. D., Leigh, R. J., Longley, I., Mahajan, A. S., Monks, P. S., Oetjen, H., Orr-Ewing, A. J., Plane, J. M.
1225 C., Potin, P., Shillings, A. J. L., Thomas, F., Von Glasow, R., Wada, R., Whalley, L. K. and Whitehead,
1226 J. D.: Iodine-mediated coastal particle formation: An overview of the Reactive Halogens in the Marine
1227 boundary layer (RHAMBLe) Roscoff coastal study, *Atmos. Chem. Phys.*, 10(6), 2975–2999,
1228 doi:10.5194/acp-10-2975-2010, 2010.
- 1229 Meixner, F. X. and Yang, W. X.: Biogenic emissions of nitric oxide and nitrous oxide from arid and semi-arid
1230 land, in *Dryland Ecohydrology.*, 2006.
- 1231 Mirme, S. and Mirme, A.: The mathematical principles and design of the NAIS - A spectrometer for the
1232 measurement of cluster ion and nanometer aerosol size distributions, *Atmos. Meas. Tech.*, 6(4), 1061–
1233 1071, doi:10.5194/amt-6-1061-2013, 2013.

1234 Nieminen, T., Asmi, A., Aalto, P. P., Keronen, P., Petäjä, T., Kulmala, M., Kerminen, V. M., Nieminen, T.
1235 and Dal Maso, M.: Trends in atmospheric new-particle formation: 16 years of observations in a boreal-
1236 forest environment, *Boreal Environ. Res.*, 19(September), 191–214, 2014.

1237 O’ Dowd, C. D., Jimenez, J. L., Bahreini, R., Flagan, R. C., Seinfeld, J. H., Hämerl, K., Pirjola, L., Kulmala,
1238 M. and Hoffmann, T.: Marine aerosol formation from biogenic iodine emissions, *Nature*, 417(6889),
1239 632–636, doi:10.1038/nature00775, 2002.

1240 Okuljar, M., Kuuluvainen, H., Kontkanen, J., Garmash, O., Olin, M., Niemi, J. V., Timonen, H., Kangasluoma,
1241 J., Tham, Y. J., Baalbaki, R., Sipilä, M., Salo, L., Lintusaari, H., Portin, H., Teinilä, K., Aurela, M., Dal
1242 Maso, M., Rönkkö, T., Petäjä, T. and Paasonen, P.: Measurement report: The influence of traffic and
1243 new particle formation on the size distribution of 1-800nm particles in Helsinki-a street canyon and an
1244 urban background station comparison, *Atmos. Chem. Phys.*, doi:10.5194/acp-21-9931-2021, 2021.

1245 Olin, M., Kuuluvainen, H., Aurela, M., Kalliokoski, J., Kuittinen, N., Isotalo, M., Timonen, H. J., Niemi, J.
1246 V., Rönkkö, T. and Dal Maso, M.: Traffic-originated nanocluster emission exceeds H₂SO₄-driven
1247 photochemical new particle formation in an urban area, *Atmos. Chem. Phys.*, 20(1), 1–13,
1248 doi:10.5194/acp-20-1-2020, 2020.

1249 Paasonen, P., Nieminen, T., Asmi, E., Manninen, H. E., Petäjä, T., Plass-Dülmer, C., Flentje, H., Birmili, W.,
1250 Wiedensohler, A., Hörrak, U., Metzger, A., Hamed, A., Laaksonen, A., Facchini, M. C., Kerminen, V.
1251 M. and Kulmala, M.: On the roles of sulphuric acid and low-volatility organic vapours in the initial steps
1252 of atmospheric new particle formation, *Atmos. Chem. Phys.*, 10(22), 11223–11242, doi:10.5194/acp-
1253 10-11223-2010, 2010.

1254 Peters, C., Pechtl, S., Stutz, J., Hebestreit, K., Hönninger, G., Heumann, K. G., Schwarz, A., Winterlik, J. and
1255 Platt, U.: Reactive and organic halogen species in three different European coastal environments, *Atmos.*
1256 *Chem. Phys.*, 5(12), 3357–3375, doi:10.5194/acp-5-3357-2005, 2005.

1257 Pierce, J. R., Riipinen, I., Kulmala, M., Ehn, M., Petäjä, T., Junninen, H., Worsnop, D. R. and Donahue, N.
1258 M.: Quantification of the volatility of secondary organic compounds in ultrafine particles during
1259 nucleation events, *Atmos. Chem. Phys.*, 11(17), 9019–9036, doi:10.5194/acp-11-9019-2011, 2011.

1260 Raso, A. R. W., Custard, K. D., May, N. W., Tanner, D., Newburn, M. K., Walker, L., Moore, R. J., Huey, L.
1261 G., Alexander, L., Shepson, P. B. and Pratt, K. A.: Active molecular iodine photochemistry in the Arctic,
1262 *Proc. Natl. Acad. Sci. U. S. A.*, 114(38), 10053–10058, doi:10.1073/pnas.1702803114, 2017.

1263 Riipinen, I., Yli-Juuti, T., Pierce, J. R., Petäjä, T., Worsnop, D. R., Kulmala, M. and Donahue, N. M.: The
1264 contribution of organics to atmospheric nanoparticle growth, *Nat. Geosci.*, 5(7), 453–458,
1265 doi:10.1038/ngeo1499, 2012.

1266 Riipinen, I., Yli-Juuti, T., Pierce, J. R., Petäjä, T., Worsnop, D. R., Kulmala, M. and Donahue, N. M.: The
1267 contribution of organics to atmospheric nanoparticle growth, *Nat. Geosci.*, doi:10.1038/ngeo1499,
1268 2012b.

1269 Rong, H., Liu, J., Zhang, Y., Du, L., Zhang, X. and Li, Z.: Nucleation mechanisms of iodic acid in clean and
1270 polluted coastal regions, *Chemosphere*, 253, 126743, doi:10.1016/j.chemosphere.2020.126743, 2020.

- 1271 Rose, C., Zha, Q., Dada, L., Yan, C., Lehtipalo, K., Junninen, H., Mazon, S. B., Jokinen, T., Sarnela, N., Sipilä,
1272 M., Petäjä, T., Kerminen, V. M., Bianchi, F. and Kulmala, M.: Observations of biogenic ion-induced
1273 cluster formation in the atmosphere, *Sci. Adv.*, 4(4), 1–11, doi:10.1126/sciadv.aar5218, 2018.
- 1274 Saiz-Lopez, A. and Plane, J. M. C.: Novel iodine chemistry in the marine boundary layer, *Geophys. Res. Lett.*,
1275 31(4), 1999–2002, doi:10.1029/2003GL019215, 2004.
- 1276 Saiz-Lopez, A., Plane, J. M. C., Baker, A. R., Carpenter, L. J., Von Glasow, R., Gómez Martín, J. C.,
1277 McFiggans, G. and Saunders, R. W.: Atmospheric chemistry of iodine, *Chem. Rev.*, 112(3), 1773–1804,
1278 doi:10.1021/cr200029u, 2012.
- 1279 Schade, G. W. and P. J. Crutzen.: Emission of aliphatic-amines from animal husbandry and their reactions:
1280 Potential source of N₂O and HCN, *J. Atmos. Chem.*, 22(3), 319–346, doi:10.1007/BF00696641, 1995.
- 1281 Schagerström, E., Forslund, H., Kautsky, L., Pärnoja, M. and Kotta, J.: Does thalli complexity and biomass
1282 affect the associated flora and fauna of two co-occurring *Fucus* species in the Baltic Sea?, *Estuar. Coast.*
1283 *Shelf Sci.*, doi:10.1016/j.ecss.2014.08.022, 2014.
- 1284 Sipilä, M., Sarnela, N., Jokinen, T., Junninen, H., Hakala, J., Rissanen, M. P., Praplan, A., Simon, M.,
1285 Kürten, A., Bianchi, F., Dommen, J., Curtius, J., Petäjä, T., and Worsnop, D. R.: Bisulfate – cluster
1286 based atmospheric pressure chemical ionization mass spectrometer for high-sensitivity (< 100 ppqV)
1287 detection of atmospheric dimethyl amine: proof-of-concept and first ambient data from boreal forest,
1288 *Atmos. Meas. Tech.*, 8, 4001–4011, <https://doi.org/10.5194/amt-8-4001-2015>, 2015.
- 1289 Sipila, M., Berndt, T., Petaja, T., Brus, D., Vanhanen, J., Stratmann, F., Patokoski, J., Mauldin, R. L.,
1290 Hyvärinen, A. P., Lihavainen, H. and Kulmala, M.: The role of sulfuric acid in atmospheric nucleation,
1291 *Science* (80-.), 327(5970), 1243–1246, doi:10.1126/science.1180315, 2010.
- 1292 Sipilä, M.: Insights Into Atmospheric Nucleation. [online] Available from:
1293 <https://helda.helsinki.fi/bitstream/handle/10138/154171/insights.pdf?sequence=1>, 2010.
- 1294 Sipilä, M., Sarnela, N., Jokinen, T., Henschel, H., Junninen, H., Kontkanen, J., Richters, S., Kangasluoma, J.,
1295 Franchin, A., Peräkylä, O., Rissanen, M. P., Ehn, M., Vehkamäki, H., Kurten, T., Berndt, T., Petäjä, T.,
1296 Worsnop, D., Ceburnis, D., Kerminen, V. M., Kulmala, M. and O’Dowd, C.: Molecular-scale evidence
1297 of aerosol particle formation via sequential addition of HIO₃, *Nature*, 537(7621), 532–534,
1298 doi:10.1038/nature19314, 2016.
- 1299 Steinke, M., Hodapp, B., Subhan, R., Bell, T. G. and Martin-Creuzburg, D.: Flux of the biogenic volatiles
1300 isoprene and dimethyl sulfide from an oligotrophic lake, *Sci. Rep.*, doi:10.1038/s41598-017-18923-5,
1301 2018.
- 1302 Stolzenburg, D., Stolzenburg, D., Simon, M., Ranjithkumar, A., Kürten, A., Lehtipalo, K., Lehtipalo, K.,
1303 Gordon, H., Ehrhart, S., Finkenzeller, H., Pichelstorfer, L., Nieminen, T., He, X. C., Brilke, S., Xiao,
1304 M., Amorim, A., Baalbaki, R., Baccarini, A., Beck, L., Bräkling, S., Murillo, L. C., Chen, D., Chu, B.,
1305 Dada, L., Dias, A., Dommen, J., Duplissy, J., El Haddad, I., Fischer, L., Carracedo, L. G., Heinritzi, M.,
1306 Kim, C., Kim, C., Koenig, T. K., Kong, W., Lamkaddam, H., Lee, C. P., Leiminger, M., Leiminger, M.,
1307 Li, Z., Makhmutov, V., Manninen, H. E., Marie, G., Marten, R., Müller, T., Nie, W., Partoll, E., Petäjä,

1308 T., Pfeifer, J., Philippov, M., Rissanen, M. P., Rissanen, M. P., Rörup, B., Schobesberger, S.,
1309 Schuchmann, S., Shen, J., Sipilä, M., Steiner, G., Stozhkov, Y., Tauber, C., Tham, Y. J., Tomé, A.,
1310 Vazquez-Pufleau, M., Wagner, A. C., Wagner, A. C., Wang, M., Wang, Y., Weber, S. K., Wimmer, D.,
1311 Wimmer, D., Wlasits, P. J., Wu, Y., Ye, Q., Zauner-Wieczorek, M., Baltensperger, U., Carslaw, K. S.,
1312 Curtius, J., Donahue, N. M., Flagan, R. C., Hansel, A., Hansel, A., Kulmala, M., Lelieveld, J., Volkamer,
1313 R., Kirkby, J., Kirkby, J. and Winkler, P. M.: Enhanced growth rate of atmospheric particles from
1314 sulfuric acid, *Atmos. Chem. Phys.*, doi:10.5194/acp-20-7359-2020, 2020.

1315 Suikkanen, S., Laamanen, M. and Huttunen, M.: Long-term changes in summer phytoplankton communities
1316 of the open northern Baltic Sea, *Estuar. Coast. Shelf Sci.*, 71(3–4), 580–592,
1317 doi:10.1016/j.ecss.2006.09.004, 2007.

1318 Suikkanen, S., Pulina, S., Engström-Öst, J., Lehtiniemi, M., Lehtinen, S. and Brutemark, A.: Climate Change
1319 and Eutrophication Induced Shifts in Northern Summer Plankton Communities, *PLoS One*, 8(6), 1–10,
1320 doi:10.1371/journal.pone.0066475, 2013.

1321 SYKE press release (29 August 2019), Summary of algal bloom monitoring June–August 2019: Cyanobacteria
1322 were mostly mixed in the water in the Finnish sea areas, in lakes the cyanobacteria situation varied a lot.
1323 [https://www.syke.fi/enUS/Current/Press_releases/Summary_of_algal_bloom_monitoring_JuneAu\(513](https://www.syke.fi/enUS/Current/Press_releases/Summary_of_algal_bloom_monitoring_JuneAu(513)
1324 [91\)](https://www.syke.fi/enUS/Current/Press_releases/Summary_of_algal_bloom_monitoring_JuneAu(513).

1325 Torn, K., Krause-Jensen, D. and Martin, G.: Present and past depth distribution of bladderwrack (*Fucus*
1326 *vesiculosus*) in the Baltic Sea, *Aquat. Bot.*, 84(1), 53–62, doi:10.1016/j.aquabot.2005.07.011, 2006.

1327 Väkevä, M., Hämeri, K., Puhakka, T., Nilsson, E. D., Hohti, H. and Mäkelä, J. M.: Effects of meteorological
1328 processes on aerosol particle size distribution in an urban background area, *J. Geophys. Res. Atmos.*,
1329 105(D8), 9807–9821, doi:10.1029/1999JD901143, 2000.

1330 Vanhanen, J., Mikkilä, J., Lehtipalo, K., Sipilä, M., Manninen, H. E., Siivola, E., Petäjä, T. and Kulmala, M.:
1331 Particle size magnifier for nano-CN detection, *Aerosol Sci. Technol.*, 45(4), 533–542,
1332 doi:10.1080/02786826.2010.547889, 2011.

1333 Wagner, R., Manninen, H.E., Franchin, A., Lehtipalo, K., Mirme, S., Steiner, G., Petäjä, T., Kulmala,
1334 M.: On the accuracy of ion measurements using a Neutral cluster and Air Ion Spectrometer, *Boreal*
1335 *Environ. Res.*, 21, pp. 230-241, 2016.

1336 Wang, Z., Wu, Z., Yue, D., Shang, D., Guo, S., Sun, J., Ding, A., Wang, L., Jiang, J., Guo, H., Gao, J., Cheung,
1337 H. C., Morawska, L., Keywood, M. and Hu, M.: New particle formation in China: Current knowledge
1338 and further directions, *Sci. Total Environ.*, doi:10.1016/j.scitotenv.2016.10.177, 2017.

1339 Wang, Z. B., Hu, M., Yue, D. L., Zheng, J., Zhang, R. Y., Wiedensohler, A., Wu, Z. J., Nieminen, T. and Boy,
1340 M.: Evaluation on the role of sulfuric acid in the mechanisms of new particle formation for Beijing case,
1341 *Atmos. Chem. Phys.*, 11(24), 12663–12671, doi:10.5194/acp-11-12663-2011, 2011.

1342 Weber, R. J., McMurry, P. H., Mauldin, L., Tanner, D. J., Eisele, F. L., Brechtel, F. J., Kreidenweis, S. M.,
1343 Kok, G. L., Schillawski, R. D. and Baumgardner, B.: A study of new particle formation and growth
1344 involving biogenic and trace gas species measured during ACE 1, *J. Geophys. Res. Atmos.*, 103(D13),

1345 16385–16396, doi:10.1029/97JD02465, 1998.

1346 Weber, R. J., McMurry, P. H., Mauldin, R. L., Tanner, D. J., Eisele, F. L., Clarke, A. D. and Kapustin, V. N.:
1347 New particle formation in the remote troposphere: A comparison of observations at various sites,
1348 *Geophys. Res. Lett.*, 26(3), 307–310, doi:10.1029/1998GL900308, 1999.

1349 Wimmer, D., Buenrostro Mazon, S., Elina Manninen, H., Kangasluoma, J., Franchin, A., Nieminen, T.,
1350 Backman, J., Wang, J., Kuang, C., Krejci, R., Brito, J., Goncalves Morais, F., Turnbull Martin, S.,
1351 Artaxo, P., Kulmala, M., Kerminen, V. M. and Petäjä, T.: Ground-based observation of clusters and
1352 nucleation-mode particles in the Amazon, *Atmos. Chem. Phys.*, 18(17), 13245–13264, doi:10.5194/acp-
1353 18-13245-2018, 2018.

1354 Yan, C., Yin, R., Lu, Y., Dada, L., Yang, D., Fu, Y., Kontkanen, J., Deng, C., Garmash, O., Ruan, J., Baalbaki,
1355 R., Schervish, M., Cai, R., Bloss, M., Chan, T., Chen, T., Chen, Q., Chen, X., Chen, Y., Chu, B.,
1356 Dällenbach, K., Foreback, B., He, X., Heikkinen, L., Jokinen, T., Junninen, H., Kangasluoma, J.,
1357 Kokkonen, T., Kurppa, M., Lehtipalo, K., Li, H., Li, H., Li, X., Liu, Y., Ma, Q., Paasonen, P., Rantala,
1358 P., Pileci, R. E., Rusanen, A., Sarnela, N., Simonen, P., Wang, S., Wang, W., Wang, Y., Xue, M., Yang,
1359 G., Yao, L., Zhou, Y., Kujansuu, J., Petäjä, T., Nie, W., Ma, Y., Ge, M., He, H., Donahue, N. M.,
1360 Worsnop, D. R., Veli-Matti, K., Wang, L., Liu, Y., Zheng, J., Kulmala, M., Jiang, J. and Bianchi, F.:
1361 The Synergistic Role of Sulfuric Acid, Bases, and Oxidized Organics Governing New-Particle
1362 Formation in Beijing, *Geophys. Res. Lett.*, doi:10.1029/2020GL091944, 2021.

1363 Yao, L., Garmash, O., Bianchi, F., Zheng, J., Yan, C., Kontkanen, J., Junninen, H., Mazon, S. B., Ehn, M.,
1364 Paasonen, P., Sipilä, M., Wang, M., Wang, X., Xiao, S., Chen, H., Lu, Y., Zhang, B., Wang, D., Fu, Q.,
1365 Geng, F., Li, L., Wang, H., Qiao, L., Yang, X., Chen, J., Kerminen, V. M., Petäjä, T., Worsnop, D. R.,
1366 Kulmala, M. and Wang, L.: Atmospheric new particle formation from sulfuric acid and amines in a
1367 Chinese megacity, *Science* (80-.), 361(6399), 278–281, doi:10.1126/science.aao4839, 2018.

1368 Yu, H., Ren, L., Huang, X., Xie, M., He, J. and Xiao, H.: Iodine speciation and size distribution in ambient
1369 aerosols at a coastal new particle formation hotspot in China, *Atmos. Chem. Phys.*, doi:10.5194/acp-19-
1370 4025-2019, 2019.

1371 Zhang, R., Wang, L., Khalizov, A. F., Zhao, J., Zheng, J., McGraw, R. L. and Molina, L. T.: Formation of
1372 nanoparticles of blue haze enhanced by anthropogenic pollution, *Proc. Natl. Acad. Sci. U. S. A.*,
1373 106(42), 17650–17654, doi:10.1073/pnas.0910125106, 2009.

1374 Zheng, G., Kuang, C., Uin, J., Watson, T. and Wang, J.: Large contribution of organics to condensational
1375 growth and formation of cloud condensation nuclei (CCN) in the remote marine boundary layer, *Atmos.*
1376 *Chem. Phys.*, doi:10.5194/acp-20-12515-2020, 2020.